Observability Analysis and Filter Design for the Orion Earth-Moon Attitude Filter

Renato Zanetti[1] and Christopher N. D'Souza[2]
NASA Johnson Space Center, Houston, Texas, 77058

The Orion attitude navigation design is presented, together with justification of the choice of states in the filter and an analysis of the observability of its states while processing star tracker measurements. The analysis shows that when the gyro biases and scale factors drift at different rates and are modeled as first-order Gauss-Markov processes, the states are observable so long as the time constants are not the same for both sets of states. In addition, the IMU-to-Star Tracker misalignments are modeled as first-order Gauss-Markov processes and these states are estimated. These results are used to finalize the design of the attitude estimation algorithm and the attitude calibration maneuvers.

I. Introduction

A variety of attitude estimation designs have been presented in the literature. Ref [1] provides an overview of nonlinear attitude estimation methods. Two main approaches for Kalman-like estimation algorithms are the additive extended Kalman filter [2] and the multiplicative extended Kalman filter (MEKF) [3]. Specialized estimators exists for particular classes of problems, for example magnetometer-only attitude determination [4] or angles-only attitude determination [5]. In this work quaternion "measurements" from the star tracker are processed by the filter; some algorithm derived from the Denvenport's q-method [6] is used in the star tracker firmware to produce a quaternion, hence the q-method effectively functions as a preprocessor feeding the attitude filter [7].

After a successful completion of Exploration Flight Test 1 on December 5, 2014, NASA's Orion vehicle next two missions are schedule to take the vehicle back to Moon. Exploration Mission 1 (EM1) is currently

---

[1] GN&C Autonomous Flight Systems Engineer, Aeroscience and Flight Mechanics Division, AIAA Senior Member.
[2] GN&C Autonomous Flight Systems Engineer, Aeroscience and Flight Mechanics Division. AIAA Associate Fellow.

scheduled for a 2018 launch, it is unmanned and it will encompass a distant retrograde orbit on the other side of the Moon. Exploration Mission 2 (EM2) is currently schedule for 2021 and will take astronauts in lunar orbit.

During EM 1 and 2, the primary navigation source of the Orion vehicle in cislunar space is given by ground updates provided by mission control and based on tracking the vehicle from ground stations. Attitude determination, on the other hand, is done onboard and relies on star trackers and IMUs. This paper details the design of the Orion attitude filter, which is an MEKF design. A feature of this design is that propagation of both the state and the covariance is done analytically, no numerical methods such as Runge-Kutta integrators or numerical evaluation of matrix exponentials occur. The only assumption made is that the angular velocity is constant during some small time step (1 sec). This assumption is not constraining because the propagation step can be subdivided into arbitrarily small intervals down to the inertial measurement unit (IMU) output rate (typically 200 Hertz). Modern strap-down gyros provide integrated angular velocity ($\Delta\boldsymbol{\theta}$) over a small interval, therefore assuming the angular velocity is constant over this interval is a very common approach employed in inertial navigation. Alternatively, several consecutive $\Delta\boldsymbol{\theta}$ samples can be used to approximate the angular velocity as a polynomial. This second approach inevitably introduces an additional delay into the system and it does not produce tangible benefits because of the very high output rate of modern IMUs ($>$ 200 Hz).

A contribution of this work is a detailed analysis of the observability of the star tracker misalignments, gyro biases and scale factors for the attitude filter. This is particularly important for the Orion vehicle in light of the fact that the star tracker is located on the Crew Module Adapter (CMA), 4.1 meters from the IMU (located on the Crew Module), and subject to flex motion due to thermal and crew module pressurization effects. The European Space Agency provides Orion's Service Module which is connected to NASA's Crew Module via the CMA; the CMA's design and performance is not completed yet. Figure 1 shows the components of the Orion vehicle. Orion does not have a navigation bench on which both the star trackers and the IMUs are mounted. Hence the Orion design needs to accommodate variable misalignments between IMUs and star trackers; furthermore the design needs to be robust to CMA misalignments which are not yet quantified and might not be until after EM1. The observability analysis is done on the linearized system; this approach has been successfully applied to angles-only navigation [8]. The angles-only navigation example shows how that

the ignored nonlinearities can make the system observable even when the linear criteria establishes it is not. It is the experience of the authors that in these situations the observability gained from the nonlinearities is so weak that effectively the uncertainty does not decrease of any appreciable amount and is typically overcome by errors due to unmodeled dynamics (process noise). An excellent reference that describes calibration of biases and misalignments of attitude sensors, as well as maneuvers needed to observe such calibration parameters, is the survey paper by Pittelkau [9]. Detailed analysis of the observability of gyro errors as well as persistence of excitation and calibration maneuvers needed to estimate them is found in Ref. [10].

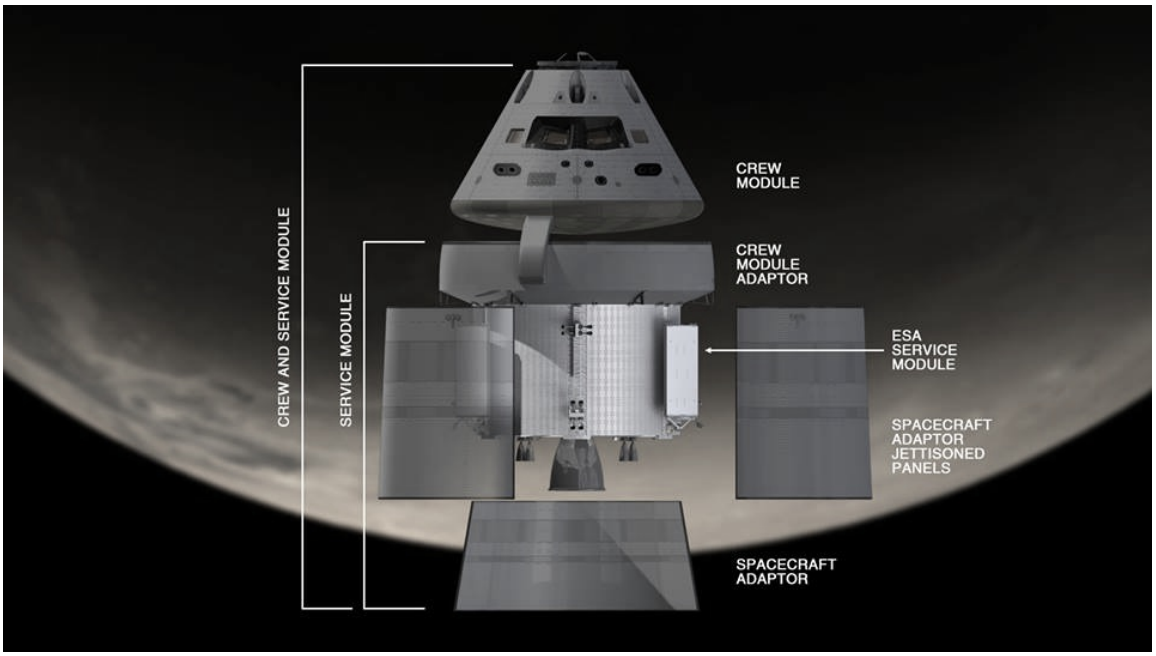

Fig. 1 Orion Components Including Crew Module and Crew Module Adapter, Credit: NASA

II. The Analysis Model

A three-dimensional parameterization of attitude is the so-called rotation vector $\boldsymbol{\phi}$ [11] that has kinematics (usually attributed to Bortz [12]) given by

$$\dot{\boldsymbol{\phi}} = \boldsymbol{\omega} - \frac{1}{2}\boldsymbol{\omega} \times \boldsymbol{\phi} + \left[1 - \frac{\phi \sin\phi}{2(1-\cos\phi)}\right] \frac{\boldsymbol{\phi} \times \boldsymbol{\phi} \times \boldsymbol{\omega}}{\phi^2}, \qquad \phi = \|\boldsymbol{\phi}\| \tag{1}$$

The cross product matrix is defined as

$$[\mathbf{v}\times] \triangleq \begin{bmatrix} 0 & -v_3 & v_2 \\ v_3 & 0 & -v_1 \\ -v_2 & v_1 & 0 \end{bmatrix}$$

The gyro measurement is given by

$$\boldsymbol{\omega}_m = (I_3 + [\mathbf{s_g}\backslash])\,\boldsymbol{\omega} + \mathbf{b} + \boldsymbol{\nu} \tag{2}$$

where $\mathbf{b}$ is the gyro bias, $\mathbf{s_g}$ is the gyro scale factor expressed in terms of a diagonal matrix operator, I_3 is the 3×3 identity matrix, and $\boldsymbol{\nu}$ represents the angle random walk. Like the cross product operator, the diagonal operator on a vector, $\mathbf{v}$, is defined as

$$[\mathbf{v}\backslash] \triangleq \begin{bmatrix} v_1 & 0 & 0 \\ 0 & v_2 & 0 \\ 0 & 0 & v_3 \end{bmatrix}$$

and

$$\begin{aligned} [\mathbf{v}\backslash]\,\mathbf{w} &= [\mathbf{w}\backslash]\,\mathbf{v} \\ [\mathbf{v}\backslash]\,[\mathbf{w}\backslash] &= [\mathbf{w}\backslash]\,[\mathbf{v}\backslash] \end{aligned}$$

for any vectors $\mathbf{v}$ and $\mathbf{w}$.

A star tracker (ST) measurement is available and modeled with an angle bias, $\boldsymbol{\mu}$, which includes both internal measurement biases and, more importantly, misalignments with respect to the gyro. Given the following state vector

$$\mathbf{X} = \begin{bmatrix} \mathbf{a} \\ \mathbf{b} \\ \boldsymbol{\mu} \end{bmatrix} \tag{3}$$

where $\mathbf{a}$ is an MEKF attitude error parameterization [13] and the star tracker measurement residual is also expressed with a three dimensional attitude parameterization and is given by (assuming small angles)

$$\boldsymbol{\epsilon} = \mathbf{a} + \boldsymbol{\mu} + \boldsymbol{\eta} \tag{4}$$

where $\boldsymbol{\mu}$ is a misalignment (or, equivalently, a bias) and $\boldsymbol{\eta}$ is white noise. The measurement mapping matrix is

$$H = \begin{bmatrix} I_3 & O_3 & I_3 \end{bmatrix}, \tag{5}$$

where I_3 is the 3×3 identity matrix and O_3 is the 3×3 matrix of all zeros.

Given the system dynamics

$$\dot{\mathbf{x}} = F\mathbf{x} \quad \text{with } \mathbf{x}(t_0) = \mathbf{x}_0 \tag{6}$$

the state transition matrix can be expressed as

$$\dot{\Phi}(t, t_0) = F\,\Phi(t, t_0) \quad \text{with } \Phi(t_0, t_0) = I \tag{7}$$

where for constant dynamics matrix F, the state transition matrix Φ is expressed as a matrix exponential

$$\Phi(t, t_0) = \mathrm{e}^{F(t-t_0)} = I + F(t-t_0) + \frac{1}{2!}F^2(t-t_0)^2 + \frac{1}{3!}F^2(t-t_0)^3 + ... \tag{8}$$

Given a system of the form

$$\dot{\Phi}^*(t, t_0) = F\,\Phi^*(t, t_0) \quad \text{with } \Phi^*(t_0, t_0) = C \tag{9}$$

the solution is

$$\Phi^*(t, t_0) = \Phi(t, t_0)\,C = \mathrm{e}^{F(t-t_0)}\,C \tag{10}$$

which can be easily verified by substituting $\Phi^*(t, t_0)$ (found in Eq. (10)) into Eq. (9).

A. Observability Analysis

Consider the n-dimensional state $\boldsymbol{x}$ and the m-dimensional linear measurement $\boldsymbol{y}$ affected by additive noise $\boldsymbol{\eta}$.

$$\boldsymbol{y} = H\boldsymbol{x} + \boldsymbol{\eta}$$

H is the $m \times n$ measurement sensitivity matrix. For the scope of this section the weights in the least-squares solution are omitted; the results are identical in the weighted least-squares case (as long as the weighting matrices are chosen non-singular). The optimal estimate of $\boldsymbol{x}$ based on $\boldsymbol{y}$ is given by

$$\hat{\boldsymbol{x}} = H^T(HH^T)^{-1}\boldsymbol{y}$$

This system is observable when the inverse of the matrix in parenthesis exists; this condition is satisfied when $m \geq n$ and H is of full column rank (i.e. $\operatorname{rank} H = n$, this second condition implies the first). Naturally if a column of H is comprised of all zeros, the system is not observable and the component of the state vector corresponding to the zero column is not determinable from the measurement information. For example if $n = 3$ so that

$$\boldsymbol{x} = \begin{bmatrix} x_1 \\ x_2 \\ x_3 \end{bmatrix} \tag{11}$$

and $m = 4$ with

$$H = \begin{bmatrix} \boldsymbol{h}_1 & \mathbf{0} & \boldsymbol{h}_3 \end{bmatrix} \tag{12}$$

where $\boldsymbol{h}_i$ are 4-vectors; it follows that

$$\boldsymbol{y} = x_1\boldsymbol{h}_1 + x_3\boldsymbol{h}_3 + \boldsymbol{\eta} \tag{13}$$

clearly x_2 is not observable, it does not affect the measurement therefore cannot be inferred from it.

Assume the state vector $\boldsymbol{x}$ is partitioned in three vector components

$$\boldsymbol{x} = \begin{bmatrix} \boldsymbol{x}_1 \\ \boldsymbol{x}_2 \\ \boldsymbol{x}_3 \end{bmatrix} \tag{14}$$

assume also H is rank deficient and all vectors $\boldsymbol{v}$ in the null space of H (i.e. $H\boldsymbol{v} = \mathbf{0}$) are of the form

$$\boldsymbol{v} = \kappa \begin{bmatrix} \boldsymbol{w} \\ -A\boldsymbol{w} \\ \mathbf{0} \end{bmatrix} \tag{15}$$

where κ is some scalar, $\boldsymbol{w}$ is a unit vector with the same dimension as $\boldsymbol{x}_1$, and A is a matrix of appropriate dimensions. Under these assumptions it follows that $\boldsymbol{x}_1$ and $\boldsymbol{x}_2$ are not individually observable but $A\boldsymbol{x}_1 + \boldsymbol{x}_2$ is. More precisely, the components of $A\boldsymbol{x}_1$ and $\boldsymbol{x}_2$ that are not observable are those in the direction of $\boldsymbol{w}$. Demonstrating this proposition is quite simple. Define the following invertible matrix V

$$\boldsymbol{x}' = \begin{bmatrix} \boldsymbol{x}'_1 \\ \boldsymbol{x}'_2 \\ \boldsymbol{x}'_3 \end{bmatrix} = V\boldsymbol{x} = \begin{bmatrix} R & O & O \\ A & I & O \\ O & O & I \end{bmatrix} \boldsymbol{x} = \begin{bmatrix} R\boldsymbol{x}_1 \\ A\boldsymbol{x}_1 + \boldsymbol{x}_2 \\ \boldsymbol{x}_3 \end{bmatrix} \tag{16}$$

matrix R is a rotation matrix such that $R\boldsymbol{w} = \boldsymbol{e}_1$, where $\boldsymbol{e}_1$ is the first element of the canonical base. The inverse of V is given by

$$V^{-1} = \begin{bmatrix} R^T & O & O \\ -A\,R^T & I & O \\ O & O & I \end{bmatrix} \tag{17}$$

hence

$$0 = H\boldsymbol{v} = HV^{-1}V\boldsymbol{v} = H' \begin{bmatrix} \boldsymbol{e}_1 \\ \mathbf{0} \\ \mathbf{0} \end{bmatrix}. \tag{18}$$

This last equation informs us that $\boldsymbol{x}_2' = A\boldsymbol{x}_1 + \boldsymbol{x}_2$ is observable, while the first component of $\boldsymbol{x}'$ is not, that is to say the component of $\boldsymbol{x}_1$ parallel to $\boldsymbol{w}$ is not observable. Repeating the same analysis with

$$\boldsymbol{x}'' = \begin{bmatrix} RA^\dagger \boldsymbol{x}_2 \\ A\boldsymbol{x}_1 + \boldsymbol{x}_2 \\ \boldsymbol{x}_3 \end{bmatrix} \tag{19}$$

where "$\dagger$" represents the pseudo inverse such that $A^\dagger A\boldsymbol{z} = \boldsymbol{z},\ \forall \boldsymbol{z}$, shows that $\boldsymbol{x}_2$ is non-observable along the direction of $A\boldsymbol{w}$.

When measurements $\boldsymbol{y}_1$, $\boldsymbol{y}_2$, etc. are available at different times t_1, t_2, ..., and the state is estimated at time t_0, the procedure is the same as above but H is replaced by an augmented measurement mapping matrix constructed as [14]

$$\Lambda = \begin{bmatrix} H_1\Phi(t_1, t_0) \\ H_2\Phi(t_2, t_0) \\ \cdots \\ H_M\Phi(t_M, t_0) \end{bmatrix} \tag{20}$$

For a linear time invariant system, Λ being full rank in Eq. (20) is the usual condition to guarantee observability.

III. Observability During Coasts

This section analyzes the observability of the states in the absence of attitude maneuvers. While it is shown that modeling the non-attitude states as first order Gauss-Markov processes makes the systems

theoretically observable, the observability is weak for large Gauss-Markov time constants. During coasts, where $\boldsymbol{\omega} \approx \mathbf{0}$, given the state vector Eq. (3) the dynamics partial matrix, F is

$$F = \begin{bmatrix} O_3 & -I_3 & O_3 \\ O_3 & O_3 & O_3 \\ O_3 & O_3 & O_3 \end{bmatrix} \tag{21}$$

and the resulting state transition matrix is

$$\Phi(t+\Delta t, t) = I_3 + F\Delta t + \frac{1}{2}F^2\Delta t^2 + \cdots = \begin{bmatrix} I_3 & -I_3\Delta t & O_3 \\ O_3 & I_3 & O_3 \\ O_3 & O_3 & I_3 \end{bmatrix} \tag{22}$$

Therefore, $H(t)\Phi(t, t_0)$ is

$$H(t)\Phi(t, t_0) = \begin{bmatrix} I_3 & -I_3\,(t - t_0) & I_3 \end{bmatrix} \tag{23}$$

Analyzing the observability of the system by processing a batch of measurements provides useful insights. The batch of measurements produce a solution for the estimated state $\hat{\mathbf{x}}(0)$ if and only if

$$\operatorname{rank}(\Lambda) = \operatorname{rank} \begin{bmatrix} H \\ H\Phi(t_1, t_0) \\ \vdots \\ H\Phi(t_{n-1}, t_0) \end{bmatrix} = n \tag{24}$$

Appling this to the ST/gyro full-state observability during coast conundrum, it follows that

$$\operatorname{rank}(\Lambda) = \operatorname{rank} \begin{bmatrix} I_3 & O_3 & I_3 \\ I_3 & -I\,(t_1 - t_0) & I_3 \\ I_3 & -I\,(t_2 - t_0) & I_3 \end{bmatrix} = 6 \tag{25}$$

which is rank deficient. This confirms the lack of observability of the gyro bias, star tracker misalignments and the attitude during coasts, adding more measurements will not make the system observable. For any 3-dimensional vectors $\boldsymbol{w}$

$$\Lambda \begin{bmatrix} \boldsymbol{w} \\ \mathbf{0} \\ -\boldsymbol{w} \end{bmatrix} = 0 \tag{26}$$

which means the attitude error is not distinguishable from the star tracker misalignment in any direction, their sum is observable but their individual values are not. This insight, while previously known, is important for the design of the Orion attitude filter. Since the star tracker is mounted on the CMA, its misalignment with respect to the IMU is going to vary during flight due to flexible motion, thermal expansion, thruster firings, etc. At this point in time it is not clear the amount of flex the system will experience, nor the time constants that will govern the motion of the CMA with respect to the crew module. During long coast periods, as the alignment between IMU and star tracker changes, the estimation algorithm is not able to distinguish between them, as a consequence the attitude estimate degrades and becomes biased by the same amount of the misalignment change. A well-tuned filter will recognize such a behavior and produce an estimation error covariance consistent with the greater uncertainty. To tune the filter it is necessary to correctly model the dynamics of the relative alignment; however, due to the complexity and uncertainty of the system, producing a fully representative model is challenging and will be achieved only after flight data is collected during the first exploration mission. Since the filter cannot distinguish between the two quantities it applies the measurement correction based on its knowledge of the relative uncertainty between the two. Hence, mis-modeling the alignment uncertainty could result in the filter erroneously applying the measurement update. To avoid this potential issue, the Orion attitude filter will not process star tracker measurements during long coast periods. This decision will be re-evaluated after alignment data is collected from EM1 which will allow for better knowledge of the dynamics of the alignment between the IMU and star tracker.

Notice that process noise is not included into this analysis. Process noise causes past measurements to be de-weighted with respect to more current measurements. This fact does not change the theoretical observability of the linear systems.

Consider a linear system with $H = \begin{bmatrix} 1 & 1 \end{bmatrix}$ and measurement error variance $R = 1$, in the absence of dynamics, the two states cannot be distinguished from each other since their sum is measured. Assume the initial state estimate has estimation error covariance given by $P_0 = I_2$. Processing the measurement the updated covariance becomes

$$P_1 = \begin{bmatrix} 2/3 & -1/3 \\ -1/3 & 2/3 \end{bmatrix}$$

therefore the correlation coefficient between the two elements of the state vectors jumps from 0 to -0.5. If

another independent, identically distributed (iid) measurement becomes available, the covariance after the second update is

$$P_2 = \begin{bmatrix} 3/5 & -2/5 \\ -2/5 & 3/5 \end{bmatrix}$$

and the correlation coefficients becomes -2/3. Another update and the diagonals of the covariance become 4/7 and correlation coefficient becomes -3/4. Another update and the diagonals are 5/9 and the coefficient -4/5. Then 6/11 and -5/6, followed by 7/13 and -6/7, and so on. After enough measurements the correlation coefficient approaches -1 and the covariance approaches

$$P_n = \begin{bmatrix} 1/2 & -1/2 \\ -1/2 & 1/2 \end{bmatrix}$$

from this point on, further measurements will not produce any improvement since

$$K = HP^T/(HPH^T + R) = \begin{bmatrix} 0 \\ 0 \end{bmatrix}$$

the effects of the non-observable system are now clear, in the absence of process noise, an infinite number of measurements does not result in zero uncertainty, rather results in the states being completely correlated. Since the measurements are iid, the covariance after n updates is given by

$$P_n = P_0 - P_0H(HP_0H^T + \frac{1}{n}R)^{-1}H^TP_0 \tag{27}$$

$$\lim_{n\to+\infty} P_n = P_0 - P_0H(HP_0H^T)^{-1}H^TP_0 \tag{28}$$

Eq. (28) simply states that in the absence of process noise all the measurement noise eventually averages out, and therefore the system is equivalent to processing a single perfect measurement. Three cases may arise. If H is not of full row rank a steady state solution does not exist. This makes sense because a non-full-rank H implies that the measurements are linear combinations of each other, a solution is not possible when measurements are perfect and combinations of each other. The second case is when H is square and full rank (i.e. invertible), in this case $\lim_{n\to+\infty} P_n = O$ (the proof can be done by first showing that $\lim_{n\to+\infty} HP_nH^T = O$). Finally when H is of full row rank but not square $\lim_{n\to+\infty} HP_nH^T = O$ but this does not imply $\lim_{n\to+\infty} P_n = O$.

In general, when the system is observable, the algebraic Riccati equation has at least one finite solution (the weaker condition of detectability is sufficient [15]) even in the presence of process noise (the system

subject to process noise needs to be stabilizable for the solution to be unique). The quantity $H\mathbf{x}$ is always observable because is measured directly, hence $\lim_{n\to+\infty} HP_nH^T$ is always finite in a LTI system. In the presence of process noise HP_nH^T converges to a finite number, however, when the system is not observable HP_nH^T could converge while individual components of P are diverging.

In order to better illustrate this consider a MEMS gyro with angular random walk (ARW) of 0.2 deg/$\sqrt{\text{hr}}$ (1σ), and bias standard deviation 0.5 deg/hr. The star tracker measurement has an accuracy of 100 arcsec (3σ) and an initial misalignment of 0.1 deg (3σ). The misalignment is randomly drifting with power spectral density 0.001 deg/$\sqrt{\text{sec}}$. The initial covariance of the 9 state filter is diagonal with initial attitude uncertainty of 0.1 deg (3σ). Figure 2 shows the performance of a multiplicative extended Kalman filter (MEKF) under this scenario. It can be seen that the attitude error uncertainty increases driven by the star tracker/IMU misalignment drift. Better modeling of the star tracker does not improve the attitude uncertainty, nor does reducing the gyro's ARW. A reduction of the ARW on the other hand does improve gyro bias estimation convergence. The performance of the estimation of the gyro bias is equivalent to that in Figure 3(b). Because of the non-observable misalignment, the attitude estimation error is significantly higher than the no-misalignment case illustrated in Figure 3. The sum of the attitude and misalignment error converges to a steady state uncertainty very similar to Figure 3(a).

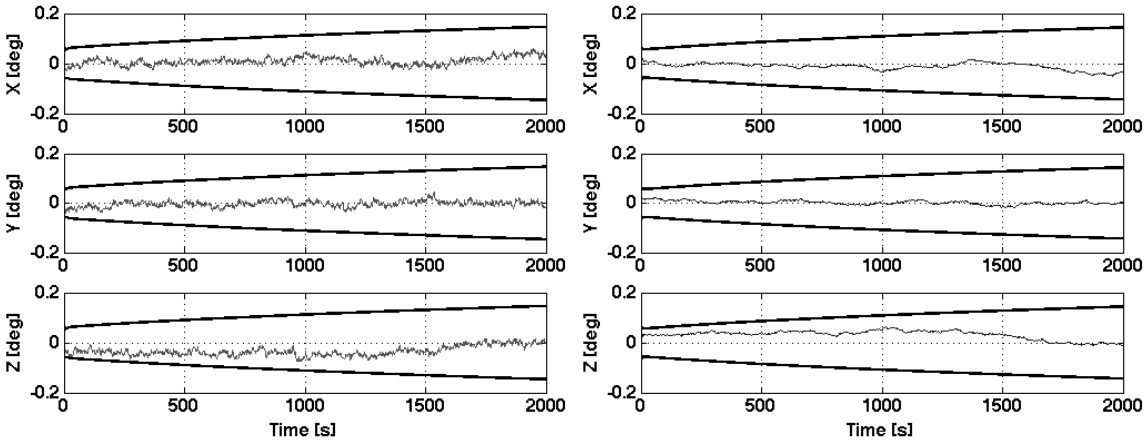

(a) Attitude Error and 3σ Predicted Uncertainty

(b) Misalignment Error and 3σ Predicted Uncertainty

Fig. 2 Estimation Error During Coast

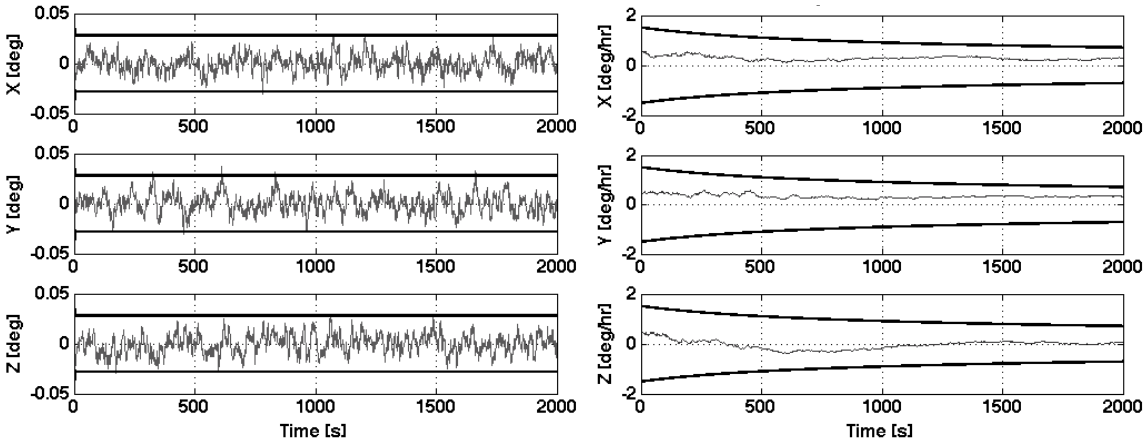

(a) Attitude Error and 3σ Predicted Uncertainty

(b) Gyro Bias Error and 3σ Predicted Uncertainty

Fig. 3 Estimation Error During Coast Without any ST/IMU Misalignment

A. Gauss-Markov Gyro Bias and ST Misalignments

Instead of modeling the gyro bias and Star Tracker misalignments as constants, they can be modeled as first-order Gauss-Markov processes. Given the state vector Eq. (3), the dynamics partial, F is

$$F = \begin{bmatrix} O_3 & -I_3 & O_3 \\ O_3 & -\frac{1}{\tau_{\mathbf{b}}} I_3 & O_3 \\ O_3 & O_3 & -\frac{1}{\tau_{\mu}} I_3 \end{bmatrix} \tag{29}$$

and the resulting state transition matrix is

$$\Phi(t,t_0) = \begin{bmatrix} I_3 & \tau_{\mathbf{b}} I_3 \left(\mathrm{e}^{-\frac{1}{\tau_{\mathbf{b}}}(t-t_0)} - 1 \right) & O_3 \\ O_3 & I_3 \mathrm{e}^{-\frac{1}{\tau_{\mathbf{b}}}(t-t_0)} & O_3 \\ O_3 & O_3 & I_3 \mathrm{e}^{-\frac{1}{\tau_{\mu}}(t-t_0)} \end{bmatrix} \tag{30}$$

With this $H(t)\Phi(t,t_0)$ is

$$H(t)\Phi(t,t_0) = \begin{bmatrix} I_3 & \tau_{\mathbf{b}} I_3 \left(\mathrm{e}^{-\frac{1}{\tau_{\mathbf{b}}}(t-t_0)} - 1 \right) & I_3 \mathrm{e}^{-\frac{1}{\tau_{\mu}}(t-t_0)} \end{bmatrix} \tag{31}$$

from which we obtain

$$\Lambda = \begin{bmatrix} I_3 & O_3 & I_3 \\ I_3 & \tau_{\mathbf{b}} I_3 \left(\mathrm{e}^{-\frac{1}{\tau_{\mathbf{b}}}(t_1-t_0)} - 1 \right) & I_3 \mathrm{e}^{-\frac{1}{\tau_{\mu}}(t_1-t_0)} \\ I_3 & \tau_{\mathbf{b}} I_3 \left(\mathrm{e}^{-\frac{1}{\tau_{\mathbf{b}}}(t_2-t_0)} - 1 \right) & I_3 \mathrm{e}^{-\frac{1}{\tau_{\mu}}(t_2-t_0)} \end{bmatrix} \tag{32}$$

Generally Λ is of full rank and hence all the states are observable. Since $exp(-(t_2 - t_0)/\tau_{\boldsymbol{\mu}}) \rightarrow 0$ as $\tau_{\boldsymbol{\mu}} \rightarrow \infty$, the system reverts to the constant-misalignment model and loses observability (in the absence of

attitude maneuvers). While under the assumption of the errors being first order Gauss-Markov processes the system is observable, in practice this observability is weak for large time constants (> 1000 sec) and is expected to be overwhelmed by process noise. Process noise degrades knowledge of the states over time, hence even an observable state can have an uncertainty that grows over time if the information gained through measurement updates is not enough to overcome the increase in uncertainty due to process noise. More importantly, in order to design an observer (or a filter), $\tau_{\boldsymbol{\mu}}$ needs to be known, which is not the case for the Orion vehicle.

IV. Observability During Attitude Maneuvers

The results of the observability analysis during coasts dictate the choice of not processing star tracker measurements during most of these epochs. This section focuses on the observability of the states while slewing the vehicle. This analysis aids the selection of the number of states in the filter. For all that follows, it is assumed that the angular velocity, $\boldsymbol{\omega}$, is constant. Typically a vehicle equipped with a reaction control system (RCS) like Orion, performs attitude maneuvers by firing the RCS jets to initiate the angular rate along the principal rotation axis, then the vehicle is controlled to slew at a constant angular velocity until the desired attitude is reached, finally the RCS jets are used to terminate the the slew.

A. Observability of Constant Gyro Bias and Star Tracker Misalignment

This sub-section assumes that the gyro bias and star-tracker-to-IMU misalignment states are (unknown) constants which are to be estimated. In such a case, given the state vector in Eq. (3), the dynamics partials are (see Ref. [16] for the kinematic equation of the MEKF attitude error [13])

$$F = \begin{bmatrix} -[\boldsymbol{\omega}_m\times] & -I_3 & O_3 \\ O_3 & O_3 & O_3 \\ O_3 & O_3 & O_3 \end{bmatrix} \tag{33}$$

The state transition matrix is given by

$$\Phi(t+\Delta t, t) = \begin{bmatrix} \Phi_{11} & \Phi_{12} & O_3 \\ O_3 & I_3 & O_3 \\ O_3 & O_3 & I_3 \end{bmatrix} \tag{34}$$

The following identities are used

$$[\boldsymbol{\omega}\times]^2 \;=\; [\boldsymbol{\omega}\times][\boldsymbol{\omega}\times] = \boldsymbol{\omega}\boldsymbol{\omega}^T - |\boldsymbol{\omega}_m|^2 I_3 \tag{35}$$

$$[\boldsymbol{\omega}\times]^{n+2} \;=\; -|\boldsymbol{\omega}_m|^2[\hat{\boldsymbol{\omega}}_m\times]^n \tag{36}$$

hence the even powers are symmetric and can be expressed in terms of $[\boldsymbol{\omega}_m\times]^2$ and the odd powers are skew symmetric and are expressed in terms of $[\boldsymbol{\omega}_m\times]$.

Using the following definitions

$$|\boldsymbol{\omega}_m| \;\triangleq\; \sqrt{\omega_x^2+\omega_y^2+\omega_z^2} \tag{37}$$

$$[\hat{\boldsymbol{\omega}}_m\times] \;\triangleq\; \frac{1}{|\boldsymbol{\omega}_m|}[\boldsymbol{\omega}_m\times] \tag{38}$$

$$\Delta\theta \;\triangleq\; |\boldsymbol{\omega}_m|\Delta t \tag{39}$$

$$\Delta t \;\triangleq\; t - t_0 \tag{40}$$

matrix Φ_{11} is given by

$$\Phi_{11}(t,t_0) \;=\; I_3 - [\hat{\boldsymbol{\omega}}_m\times]\sin\Delta\theta + [\hat{\boldsymbol{\omega}}_m\times]^2(1-\cos\Delta\theta) \tag{41}$$

which is a well known result. All the components of the state transition matrix are obtained analytically, such as

$$\Phi_{12}(t,t_0) \;=\; -\frac{1}{|\boldsymbol{\omega}_m|}\left[I_3\Delta\theta + [\hat{\boldsymbol{\omega}}_m\times](\cos\Delta\theta-1) + [\hat{\boldsymbol{\omega}}_m\times]^2(\Delta\theta-\sin\Delta\theta)\right] \tag{42}$$

which can be found in [17]

The discrete observability condition requires that

$$\Lambda = \begin{bmatrix} I_3 & O_3 & I_3 \\ \Phi_{11}(t_1,t_0) & \Phi_{12}(t_1,t_0) & I_3 \\ \Phi_{11}(t_2,t_0) & \Phi_{12}(t_2,t_0) & I_3 \end{bmatrix} \tag{43}$$

be of full rank. However Λ has rank equal to 6. Notice that $\Phi_{11}(t,t_0)\boldsymbol{\omega} = \boldsymbol{\omega}$, therefore

$$\Lambda \begin{bmatrix} \boldsymbol{\omega} \\ \mathbf{0} \\ -\boldsymbol{\omega} \end{bmatrix} = \mathbf{0} \tag{44}$$

which results in the attitude error and star tracker misalignment not being distinguishable along the direction of the constant angular velocity. Define two unit vectors $\mathbf{i}_2$ and $\mathbf{i}_3$, such that $\hat{\boldsymbol{\omega}}_m$, $\mathbf{i}_2$, and $\mathbf{i}_3$ form an orthonormal triad. Then:

$$\Phi_{12}(t,t_0)\left(|\boldsymbol{\omega}_m|\mathbf{i}_2\right) = -\left[\mathbf{i}_3(\cos\Delta\theta - 1) + \mathbf{i}_2\sin\Delta\theta\right] = -\left(\Phi_{11}(t,t_0) - I_3\right)\,\mathbf{i}_3 \tag{45}$$

therefore

$$\Lambda \begin{bmatrix} -\mathbf{i}_3 \\ |\boldsymbol{\omega}_m|\mathbf{i}_2 \\ \mathbf{i}_3 \end{bmatrix} = \mathbf{0} \tag{46}$$

hence a combination of the attitude error and misalignment in the $\mathbf{i}_3$ direction is not distinguishable from the gyro bias in the $\mathbf{i}_2$ direction. Similarly

$$\Lambda \begin{bmatrix} \mathbf{i}_2 \\ |\boldsymbol{\omega}_m|\mathbf{i}_3 \\ -\mathbf{i}_2 \end{bmatrix} = \mathbf{0} \tag{47}$$

A slew that varies the direction of the angular velocity makes the system observable. A direct consequence of this fact is that when turning to and from a maneuver execution attitude, it is desirable that Orion does not take the shortest "eigenaxis" turn, but varies the direction of the angular velocity in order to be able to estimate all components of the misalignment between star tracker and IMU. The proposed concept of operation is to slew to the maneuver attitude to gain observability and then process star tracker measurements for some time. The slew back to "tail-to-sun" also improves observability and star tracker measurements will be processed for some time during "tail-to-sun".

B. Observability of Gauss-Markov Gyro Bias and Gauss-Markov Gyro Scale Factor and Gauss-Markov Star Tracker Misalignment

This section analyzes the observability of the entire state vector during a constant angular velocity calibration maneuver when the gyro scale factor errors are estimated. An important trade is whether to include the gyro scale factor as a state in the filter; it is well known that during constant rate maneuvers the gyro scale factor cannot be discerned from the gyro bias [9]. In this sub-section it is assumed that the gyro bias and gyro scale factor states as well as the IMU/Star Tracker misalignments are first-order Gauss-Markov

processes which are to be estimated. An analytical solution to the State Transition Matrix is used which, to the best knowledge of the authors, is an original contribution of this paper. The angular velocity is given by

$$\boldsymbol{\omega}_m = (I_3 + [\mathbf{s_g}\backslash])\,\boldsymbol{\omega} + \mathbf{b} + \boldsymbol{\nu} \tag{48}$$

where $\boldsymbol{\omega}$ is the true angular velocity, $\boldsymbol{\omega}_m$ is the measured angular velocity, $\mathbf{b}$ is the gyro bias, $\mathbf{s_g}$ is the gyro scale factor and $\boldsymbol{\nu}$ represents the angle random walk. The state vector is given by

$$\mathbf{X} = \begin{bmatrix} \mathbf{a} \\ \mathbf{b} \\ \mathbf{s_g} \\ \boldsymbol{\mu} \end{bmatrix} \tag{49}$$

and the system dynamics partials are

$$F = \begin{bmatrix} -[\boldsymbol{\omega}\times] & -I_3 & -[\boldsymbol{\omega}_m\backslash] & O_3 \\ O_3 & -\frac{1}{\tau_\mathbf{b}} I_3 & O_3 & O_3 \\ O_3 & O_3 & -\frac{1}{\tau_{\mathbf{s_g}}} I_3 & O_3 \\ O_3 & O_3 & O_3 & -\frac{1}{\tau_{\boldsymbol{\mu}}} I_3 \end{bmatrix} \tag{50}$$

Φ_{11}, Φ_{12}, and Φ_{13} are required to satisfy the following equations:

$$\dot{\Phi}_{11} = -\frac{1}{2}[\boldsymbol{\omega}\times]\Phi_{11}, \qquad \text{with} \quad \Phi_{11_0} = I_3 \tag{51}$$

$$\dot{\Phi}_{12} = -\frac{1}{2}[\boldsymbol{\omega}\times]\Phi_{12} - \Phi_{22}, \qquad \text{with} \quad \Phi_{12_0} = O_3 \tag{52}$$

$$\dot{\Phi}_{13} = -\frac{1}{2}[\boldsymbol{\omega}\times]\Phi_{13} - [\boldsymbol{\omega}\backslash]\,\Phi_{33}, \quad \text{with} \quad \Phi_{13_0} = O_3 \tag{53}$$

The remaining non-zero elements of the state transition matrix are found to be:

$$\Phi_{22} = I_3 \mathrm{e}^{-\frac{t-t_0}{\tau_\mathbf{b}}} \tag{54}$$

$$\Phi_{33} = I_3 \mathrm{e}^{-\frac{t-t_0}{\tau_{\mathbf{s_g}}}} \tag{55}$$

$$\Phi_{44} = I_3 \mathrm{e}^{-\frac{t-t_0}{\tau_{\boldsymbol{\mu}}}}. \tag{56}$$

As before Φ_{11} is

$$\Phi_{11}(t, t_0) = I_3 - [\hat{\boldsymbol{\omega}}_m\times]\sin\Delta\theta + [\hat{\boldsymbol{\omega}}_m\times]^2\,(1 - \cos\Delta\theta) \tag{57}$$

The solution for Φ_{12} is given by

$$\begin{aligned}\Phi_{12}(t,t_0) &= \tau_{\mathbf{b}} I_3 \left(e^{-\frac{\Delta t}{\tau_{\mathbf{b}}}} - 1\right) - \frac{|\boldsymbol{\omega}_m|\tau_{\mathbf{b}}^2}{1+|\boldsymbol{\omega}_m|^2\tau_{\mathbf{b}}^2}[\hat{\boldsymbol{\omega}}_m\times]\left(\cos\Delta\theta - 1\right) + \frac{|\boldsymbol{\omega}_m|\tau_{\mathbf{b}}^2}{1+|\boldsymbol{\omega}_m|^2\tau_{\mathbf{b}}^2}[\hat{\boldsymbol{\omega}}_m\times]^2\sin\Delta\theta \\ &+\frac{\tau_{\mathbf{b}}}{1+|\boldsymbol{\omega}_m|^2\tau_{\mathbf{b}}^2}[\hat{\boldsymbol{\omega}}_m\times]^2\left(\cos\Delta\theta - 1\right) + \frac{\tau_{\mathbf{b}}}{1+|\boldsymbol{\omega}_m|^2\tau_{\mathbf{b}}^2}[\hat{\boldsymbol{\omega}}_m\times]\sin\Delta\theta \\ &+\frac{|\boldsymbol{\omega}_m|^2\tau_{\mathbf{b}}^3}{1+|\boldsymbol{\omega}_m|^2\tau_{\mathbf{b}}^2}[\hat{\boldsymbol{\omega}}_m\times]^2\left(e^{-\frac{\Delta t}{\tau_{\mathbf{b}}}} - 1\right) + \frac{|\boldsymbol{\omega}_m|\tau_{\mathbf{b}}^2}{1+|\boldsymbol{\omega}_m|^2\tau_{\mathbf{b}}^2}[\hat{\boldsymbol{\omega}}_m\times]\left(e^{-\frac{\Delta t}{\tau_{\mathbf{b}}}} - 1\right) \end{aligned} \tag{58}$$

Having found the solution to a matrix differential equation of the kind

$$\dot{X}(t) = AX(t) + \alpha I, \qquad X(t_0) = O \tag{59}$$

it is simple to shown that the solution to

$$\dot{Y}(t) = AY(t) + \alpha B, \qquad Y(t_0) = O \tag{60}$$

when $\dot{B} = O$, is given by

$$Y = XB. \tag{61}$$

With this in hand, the solution for Φ_{13} is easily found to be

$$\begin{aligned}\Phi_{13}(t,t_0) &= \left\{\tau_{\mathbf{s_g}} I_3 \left(e^{-\frac{\Delta t}{\tau_{\mathbf{s_g}}}} - 1\right) - \frac{|\boldsymbol{\omega}_m|\tau_{\mathbf{s_g}}^2}{1+|\boldsymbol{\omega}_m|^2\tau_{\mathbf{s_g}}^2}[\hat{\boldsymbol{\omega}}_m\times]\left(\cos\Delta\theta - 1\right) + \frac{|\boldsymbol{\omega}_m|\tau_{\mathbf{s_g}}^2}{1+|\boldsymbol{\omega}_m|^2\tau_{\mathbf{s_g}}^2}[\hat{\boldsymbol{\omega}}_m\times]^2\sin\Delta\theta \right. \\ &+\frac{\tau_{\mathbf{b}}}{1+|\boldsymbol{\omega}_m|^2\tau_{\mathbf{s_g}}^2}[\hat{\boldsymbol{\omega}}_m\times]^2\left(\cos\Delta\theta - 1\right) + \frac{\tau_{\mathbf{s_g}}}{1+|\boldsymbol{\omega}_m|^2\tau_{\mathbf{s_g}}^2}[\hat{\boldsymbol{\omega}}_m\times]\sin\Delta\theta \\ &\left.+\frac{|\boldsymbol{\omega}_m|^2\tau_{\mathbf{s_g}}^3}{1+|\boldsymbol{\omega}_m|^2\tau_{\mathbf{s_g}}^2}[\hat{\boldsymbol{\omega}}_m\times]^2\left(e^{-\frac{\Delta t}{\tau_{\mathbf{s_g}}}} - 1\right) + \frac{|\boldsymbol{\omega}_m|\tau_{\mathbf{s_g}}^2}{1+|\boldsymbol{\omega}_m|^2\tau_{\mathbf{s_g}}^2}[\hat{\boldsymbol{\omega}}_m\times]\left(e^{-\frac{\Delta t}{\tau_{\mathbf{s_g}}}} - 1\right)\right\}[\boldsymbol{\omega}_m\backslash] \end{aligned} \tag{62}$$

Of course, if $\tau_{\mathbf{s_g}} = \tau_{\mathbf{b}}$, then

$$\Phi_{13}(t,t_0) = \Phi_{12}(t,t_0)[\boldsymbol{\omega}_m\backslash] \tag{63}$$

Gyro misalignment and nonorthogonality errors are not considered in this analysis. However notice that they can both be expressed (to first order) as $\mathbf{M}(\boldsymbol{\omega})\boldsymbol{\varepsilon}$, where $\mathbf{M}(\boldsymbol{\omega})$ is a matrix function of the angular velocity and $\boldsymbol{\varepsilon}$ is the error (either misalignment or nonorthogonality). For example the contribution of the misalignment error $\boldsymbol{\mu}$ is $[\boldsymbol{\omega}\times]\boldsymbol{\mu}$, hence the state transition matrix used to calculate the attitude error generated by a misalignment is

$$\begin{aligned}\Phi_{\boldsymbol{\phi\mu}}(t,t_0) &= \left\{\tau_{\boldsymbol{\mu}_g} I_3 \left(e^{-\frac{\Delta t}{\tau_{\boldsymbol{\mu}_g}}} - 1\right) - \frac{|\boldsymbol{\omega}_m|\tau_{\boldsymbol{\mu}_g}^2}{1+|\boldsymbol{\omega}_m|^2\tau_{\boldsymbol{\mu}_g}^2}[\hat{\boldsymbol{\omega}}_m\times]\left(\cos\Delta\theta - 1\right) + \frac{|\boldsymbol{\omega}_m|\tau_{\boldsymbol{\mu}_g}^2}{1+|\boldsymbol{\omega}_m|^2\tau_{\boldsymbol{\mu}_g}^2}[\hat{\boldsymbol{\omega}}_m\times]^2\sin\Delta\theta \right. \\ &+\frac{\tau_{\mathbf{b}}}{1+|\boldsymbol{\omega}_m|^2\tau_{\boldsymbol{\mu}_g}^2}[\hat{\boldsymbol{\omega}}_m\times]^2\left(\cos\Delta\theta - 1\right) + \frac{\tau_{\boldsymbol{\mu}_g}}{1+|\boldsymbol{\omega}_m|^2\tau_{\boldsymbol{\mu}_g}^2}[\hat{\boldsymbol{\omega}}_m\times]\sin\Delta\theta \\ &\left.+\frac{|\boldsymbol{\omega}_m|^2\tau_{\boldsymbol{\mu}_g}^3}{1+|\boldsymbol{\omega}_m|^2\tau_{\boldsymbol{\mu}_g}^2}[\hat{\boldsymbol{\omega}}_m\times]^2\left(e^{-\frac{\Delta t}{\tau_{\boldsymbol{\mu}_g}}} - 1\right) + \frac{|\boldsymbol{\omega}_m|\tau_{\boldsymbol{\mu}_g}^2}{1+|\boldsymbol{\omega}_m|^2\tau_{\boldsymbol{\mu}_g}^2}[\hat{\boldsymbol{\omega}}_m\times]\left(e^{-\frac{\Delta t}{\tau_{\boldsymbol{\mu}_g}}} - 1\right)\right\}[\boldsymbol{\omega}_m\times] \end{aligned} \tag{64}$$

and the state transition matrix used to calculate the attitude error generated by gyro nonorthogonality is obtained in a similar manner

Back to the case without gyro misalignment and nonorthogonality states, matrix $H(t)\Phi(t,t_0)$ is found to be

$$H(t)\,\Phi(t,t_0) = \begin{bmatrix} \Phi_{11}(t,t_0) & \Phi_{12}(t,t_0) & \Phi_{13}(t,t_0) & \Phi_{44}(t,t_0) \end{bmatrix} \tag{65}$$

The discrete observability condition requires that

$$\Lambda = \begin{bmatrix} I_3 & O_3 & O_3 & I_3 \\ \Phi_{11}(t_1,t_0) & \Phi_{12}(t_1,t_0) & \Phi_{13}(t_1,t_0) & \Phi_{44}(t_1,t_0) \\ \Phi_{11}(t_2,t_0) & \Phi_{12}(t_2,t_0) & \Phi_{13}(t_2,t_0) & \Phi_{44}(t_2,t_0) \\ \Phi_{11}(t_3,t_0) & \Phi_{12}(t_3,t_0) & \Phi_{13}(t_3,t_0) & \Phi_{44}(t_3,t_0) \end{bmatrix} \tag{66}$$

be of rank 12. The rank of Λ was numerically confirmed to be 12 in all tested occorunces with $\boldsymbol{\omega}_m \neq 0$ and $\tau_{\mathbf{s_g}} \neq \tau_{\mathbf{b}}$. If $\tau_{\mathbf{s_g}} = \tau_{\mathbf{b}}$, then we can write Λ as

$$\Lambda = \begin{bmatrix} I_3 & O_3 & O_3 & I_3 \\ \Phi_{11}(t_1,t_0) & \Phi_{12}(t_1,t_0) & \Phi_{12}(t_1,t_0) & \Phi_{44}(t_1,t_0) \\ \Phi_{11}(t_2,t_0) & \Phi_{12}(t_2,t_0) & \Phi_{12}(t_2,t_0) & \Phi_{44}(t_2,t_0) \\ \Phi_{11}(t_3,t_0) & \Phi_{12}(t_3,t_0) & \Phi_{12}(t_3,t_0) & \Phi_{44}(t_3,t_0) \end{bmatrix} \begin{bmatrix} I_3 & O_3 & O_3 & O_3 \\ O_3 & I_3 & O_3 & O_3 \\ O_3 & O_3 & [\boldsymbol{\omega}_m\backslash] & O_3 \\ O_3 & O_3 & O_3 & I_3 \end{bmatrix} \tag{67}$$

The third column of the first matrix in Eq. (67) is identical to the second and hence the rank is, at most, 9. Notice that for any vector $\boldsymbol{v}$

$$\Lambda \begin{bmatrix} \mathbf{0} \\ [\boldsymbol{\omega}_m\backslash]\,\boldsymbol{v} \\ -\boldsymbol{v} \\ \mathbf{0} \end{bmatrix} = \mathbf{0} \tag{68}$$

which results in the gyro bias and scale factor not being individually observable while $\boldsymbol{b} + [\boldsymbol{\omega}_m\backslash]\,\boldsymbol{s}_g$ is. Typically $\tau_{\mathbf{s_g}}$ and $\tau_{\mathbf{b}}$ are both large numbers, hence the system is weakly observable, if at all. Appropriate persistence of excitation conditions will make the system observable [9]. However this analysis shows that when gyro biases and scale factors have different stability time constants (or one of them has an infinite time constant, i.e. it is random bias) then their contributions can be distinguished from each other as long as the

angular velocity has non-zero components in all three IMU sensitive axis. While a constant angular velocity with non-zero components in all three IMU axis will make the IMU error observable, the attitude error and the star tracker misalignment will not be completely distinguishable without variations in the angular velocity vector.

V. Filter Design

In the prior sections an analytical formulation for the state transition matrix was introduced, the rationale behind the decision to not process measurements during long coast segments was presented, and the observability of the states was derived. Orion will perform slews by varying the angular velocity direction in order to completely observe the sensor error states. To finalize the algorithm design an analysis of the number of states in the filter is needed, and in particular the sensitivity to the gyro scale factor errors.

A vehicle like Orion typically keeps its attitude rate within 0.025 deg/s while holding attitude and has a slew rate of less than 1 deg/s. Typical gyros for this type of applications have an angular random walk around 0.01 deg/$\sqrt{\text{hr}}$, a bias of 0.02 deg/hr, and scale factors 15 parts per million, all 1σ values. Slewing with variable angular velocity is typically not supported because it will increase complexity and fuel usage without any tangible benefits. Using the above numbers, a 1σ scale factor causes an error of $0.025\frac{15}{10^6}$deg/s $= 0.0014$ deg/hr, more than an order of magnitude less than the actual bias. This fact suggests that the gyro scale factors are candidates to be removed from the filter, sensitivity analysis is done to confirm this fact. From the observability analysis done above, the scale factors contributions can be potentially accounted for together with the gyro bias state. It might seem that this can be done when slews always occur at about the same rate and when the two quantities have similar time constants, an error budget provides the data to decide whether to keep or remove the gyro scale factors states.

Error budgets break down the contributions of all error sources to the navigation error. For this particular analysis we are interested in the contributors to the total attitude estimation error. For this analysis the initial attitude uncertainty standard deviation is 0.033 deg. The simulation runs for 1500 seconds, for the first 1200 seconds the vehicle is coasting (a nominal residual rate of 0.02 deg/s is simulated), the estimation algorithm starts processing star tracker measurements after 1100 seconds and continues until the end. The initial 1100 seconds of simulation are there to build correlations between gyro errors and attitude error. At 1200 the

vehicle starts rolling at a rate of 1 deg/s. At 1300 seconds the vehicle stops rolling and starts pitching at a rate of 1 deg/s. At 1400 seconds the vehicle returns to coasting flight. Table 1 shows the star tracker and gyro errors used in the simulation (all values are 1σ per axis). Table 2 shows the attitude error budget with contributions from measurement noise, Angular Random Walk (ARW), Misalignment Walk (MW), attitude Initial Condition, gyro bias, gyro scale factors, and misalignment initial condition. The error budget shows that the gyro scale factor contribution is as big as that of the bias. The reason for this is that during long coasts the attitude and bias errors correlate, therefore the gyro bias is estimated when star tracker measurements are processed. The gyro scale factors on the other hand, correlate with the attitude error during slews, which are relatively slow and short, therefore the scale factors are weakly observable; yet it is a significant enough contributor.

SENSOR ERROR TYPE	1σ VALUE
Star Tracker to Gyro Misalignment	0.333 deg
Misalignment Drift	0.001 deg/s
Star Tracker Measurement Noise	100 arcsec
Gyro Bias	0.01 deg/hour
Gyro Scale factor	15 ppm
Gyro Noise (ARW)	0.007 deg/$\sqrt{\text{hour}}$

Table 1 Sensors errors

In view of this fact the state in the filter as chosen as the attitude error, gyro bias, gyro scale factor, and the star tracker to gyro misalignment:

$$\hat{\mathbf{x}} = \begin{bmatrix} \hat{\mathbf{a}}^{\mathrm{T}} & \hat{\mathbf{b}}^{\mathrm{T}} & \hat{\mathbf{s}}^{\mathrm{T}} & \hat{\boldsymbol{\mu}}^{\mathrm{T}} \end{bmatrix}^{\mathrm{T}} \tag{69}$$

The filter propagates using the gyro during long coast times. Calibration maneuvers are initiated periodically to calibrate the star tracker misalignment. Some time before the calibration maneuvers and for some time after they are concluded, star tracker measurements are being processed by the filter. Measurement updates during these pre-maneuvers coast times collapse the star tracker misalignment uncertainty down to the attitude knowledge uncertainty and potentially estimate the gyro bias.

The gyro measurement $\Delta\tilde{\boldsymbol{\theta}}_j$ is a rotation vector (an integrated angular velocity compensated for coning)

Time (s)	3σ Attitude Error Contributors (deg)							
	Meas. Noise	ARW	MW	Att. IC	Bias	SF	Mis. IC	RSS
0	0	0	0	0.2997	0	0	0	0.2997
200	0	0.0148	0	0.2997	0.0050	0.0002	0	0.3001
400	0	0.0210	0	0.2997	0.0100	0.0004	0	0.3006
600	0	0.0257	0	0.2997	0.0150	0.0005	0	0.3012
800	0	0.0297	0	0.2997	0.0200	0.0007	0	0.3018
1000	0	0.0332	0	0.2997	0.0249	0.0009	0	0.3026
1100	0.0025	0.0345	0.0030	0.2967	0.0271	0.0010	0.0298	0.3015
1200	0.0110	0.0359	0.0133	0.2954	0.0295	0.0011	0.0299	0.3012
1300	0.0253	0.0184	0.0377	0.1086	0.0127	0.0054	0.0110	0.1461
1400	0.0313	0.0105	0.0487	0.0116	0.0028	0.0050	0.0012	0.0606
1500	0.0268	0.0144	0.0487	0.0106	0.0042	0.0049	0.0011	0.0590

Table 2 Attitude Error Budget

and is accumulated by the filter at the gyro output rate Δt_j as follows

$$\mathbf{q}_{accum,j} = \mathbf{q}\big(\Delta\tilde{\boldsymbol{\theta}}_j - \hat{\mathbf{b}}_k \Delta t_j\big) \otimes \mathbf{q}_{accum,j-1} \tag{70}$$

where the subscript k designates the last navigation filter call time which is at a slower rate than gyro accumulation, $\otimes$ is the quaternion multiplication such that quaternion compose in the same order as attitude matrices, and $\mathbf{q}(\cdot)$ is the function that returns a quaternion from another attitude parameterization. Eq. (70) is only valid when the gyro bias is either constant or its time constant is several orders of magnitude greater than the filter call rate, otherwise the estimated gyro bias needs to be propagated at the IMU rate as well

$$\hat{\mathbf{b}}_{kj} = e^{-\Delta t_j/\tau_\mathbf{b}} \hat{\mathbf{b}}_{kj-1} \tag{71}$$

The state transition matrix is propagated at either the fast IMU rate, Δt_j, or the slower filter call rate, Δt_k,

and is given by

$$\Phi(t_{k+1},t_k)=\begin{bmatrix} \Phi_{11}(t_{k+1},t_k) & \Phi_{12}(t_{k+1},t_k) & \Phi_{13}(t_{k+1},t_k) & O_3 \\ O_3 & e^{-\Delta t_k/\tau_{\mathbf{b}}} I_3 & O_3 & O_3 \\ O_3 & O_3 & e^{-\Delta t_k/\tau_{\mathbf{s}}} I_3 & O_3 \\ O_3 & O_3 & O_3 & e^{-\Delta t_k/\tau_{\boldsymbol{\mu}}} I_3 \end{bmatrix} \tag{72}$$

where

$$\Delta\boldsymbol{\theta}_k = \boldsymbol{\theta}\big(\mathbf{q}_{accum,k}\otimes\mathbf{q}^*_{accum,k-1}\big) \tag{73}$$

$$\Delta\theta_k = \|\Delta\boldsymbol{\theta}_k\| \tag{74}$$

$$[\hat{\boldsymbol{\omega}}_{m,k}\times] = \frac{1}{\Delta\theta_k}[\Delta\boldsymbol{\theta}_k\times] \tag{75}$$

$$\boldsymbol{\omega}_k = \Delta\boldsymbol{\theta}_k/\Delta t_k \tag{76}$$

$$\Phi_{11}(t_{k+1},t_k) = I_3 - [\hat{\boldsymbol{\omega}}_m\times]\sin\Delta\theta_k + [\hat{\boldsymbol{\omega}}_m\times]^2(1-\cos\Delta\theta_k) \tag{77}$$

and the other two components of the state transition matrix are given by Eqs. (58) and (62)

$$\begin{aligned}\Phi_{12}(t_{k+1},t_k) &= \tau_{\mathbf{b}} I_3\left(e^{-\Delta t_k/\tau_{\mathbf{b}}}-1\right) - \frac{\Delta\theta\,\tau_{\mathbf{b}}^2}{1+\Delta\theta_k^2\,\tau_{\mathbf{b}}^2}[\hat{\boldsymbol{\omega}}_{m,k}\times](\cos\Delta\theta_k-1) + \frac{\Delta\theta\,\tau_{\mathbf{b}}^2}{1+\Delta\theta_k^2\,\tau_{\mathbf{b}}^2}[\hat{\boldsymbol{\omega}}_{m,k}\times]^2\sin\Delta\theta_k \\ &+\frac{\tau_{\mathbf{b}}}{1+\Delta\theta_k^2\,\tau_{\mathbf{b}}^2}[\hat{\boldsymbol{\omega}}_{m,k}\times]^2(\cos\Delta\theta_k-1) + \frac{\tau_{\mathbf{b}}}{1+\Delta\theta_k^2\,\tau_{\mathbf{b}}^2}[\hat{\boldsymbol{\omega}}_{m,k}\times]\sin\Delta\theta_k \\ &+\frac{\Delta\theta^2\,\tau_{\mathbf{b}}^3}{1+\Delta\theta_k^2\,\tau_{\mathbf{b}}^2}[\hat{\boldsymbol{\omega}}_{m,k}\times]^2\left(e^{-\Delta t_k/\tau_{\mathbf{b}}}-1\right) + \frac{\Delta\theta\,\tau_{\mathbf{b}}^2}{1+\Delta\theta_k^2\,\tau_{\mathbf{b}}^2}[\hat{\boldsymbol{\omega}}_{m,k}\times]\left(e^{-\Delta t_k/\tau_{\mathbf{b}}}-1\right)\end{aligned} \tag{78}$$

$$\begin{aligned}\Phi_{13}(t_{k+1},t_k) &= \Big\{\tau_{\mathbf{s}} I_3\left(e^{-\Delta t_k/\tau_{\mathbf{s}}}-1\right) - \frac{\Delta\theta\,\tau_{\mathbf{s}}^2}{1+\Delta\theta_k^2\,\tau_{\mathbf{s}}^2}[\hat{\boldsymbol{\omega}}_{m,k}\times](\cos\Delta\theta_k-1) + \frac{\Delta\theta\,\tau_{\mathbf{s}}^2}{1+\Delta\theta_k^2\,\tau_{\mathbf{s}}^2}[\hat{\boldsymbol{\omega}}_{m,k}\times]^2\sin\Delta\theta_k \\ &+\frac{\Delta\theta^2\,\tau_{\mathbf{s}}^3}{1+\Delta\theta_k^2\,\tau_{\mathbf{s}}^2}[\hat{\boldsymbol{\omega}}_{m,k}\times]^2\left(e^{-\Delta t_k/\tau_{\mathbf{s}}}-1\right) + \frac{\Delta\theta\,\tau_{\mathbf{s}}^2}{1+\Delta\theta_k^2\,\tau_{\mathbf{s}}^2}[\hat{\boldsymbol{\omega}}_{m,k}\times]\left(e^{-\Delta t_k/\tau_{\mathbf{s}}}-1\right) \\ &+\frac{\tau_{\mathbf{s}}}{1+\Delta\theta_k^2\,\tau_{\mathbf{s}}^2}[\hat{\boldsymbol{\omega}}_{m,k}\times]^2(\cos\Delta\theta_k-1) + \frac{\tau_{\mathbf{s}}}{1+\Delta\theta_k^2\,\tau_{\mathbf{s}}^2}[\hat{\boldsymbol{\omega}}_{m,k}\times]\sin\Delta\theta_k\Big\}[\boldsymbol{\omega}_k\times]\end{aligned} \tag{79}$$

function $\boldsymbol{\theta}(\cdot)$ returns a rotation vector from another attitude parameterization and superscript "$*$" indicates the quaternion conjugate. The state and covariance P propagation are given by

$$\hat{\mathbf{q}}_{bi}(t_{k+1}) = \big(\mathbf{q}_{accum,k}\otimes\mathbf{q}^*_{accum,k-1}\big)\otimes\hat{\mathbf{q}}_{bi}(t_k) \tag{80}$$

$$\hat{\mathbf{b}}(t_{k+1}) = e^{-\Delta t_k/\tau_{\mathbf{b}}}\,\hat{\mathbf{b}}(t_k) \tag{81}$$

$$\hat{\mathbf{s}}(t_{k+1}) = e^{-\Delta t_k/\tau_{\mathbf{s}}}\,\hat{\mathbf{s}}(t_k) \tag{82}$$

$$\hat{\boldsymbol{\mu}}(t_{k+1}) = e^{-\Delta t_k/\tau_{\boldsymbol{\mu}}}\,\hat{\boldsymbol{\mu}}(t_k) \tag{83}$$

$$P^-_{k+1} = \Phi(t_{k+1},t_k)P^+_k\Phi(t_{k+1},t_k)^{\mathrm{T}} + \overline{Q}_k \tag{84}$$

The simplest approximation for $\overline{Q}_k$ is a single-step forward Euler integration which is expressed as

$$\overline{Q}_{k_{Euler}} = \begin{bmatrix} Q_{ARW}\Delta t_k & O & O & \\ O & \sigma^2_{\mathbf{bb}}(1-e^{-2\Delta t_k/\tau_\mathbf{b}})I & O & O \\ O & O & \sigma^2_{\mathbf{ss}}(1-e^{-2\Delta t_k/\tau_\mathbf{s}})\mathbf{I} & O \\ O & O & O & \sigma^2_{\boldsymbol{\mu\mu}}(1-e^{-2\Delta t_k/\tau_\mu})I \end{bmatrix} \tag{85}$$

where Q_{ARW} is the gyro angular random walk and $\sigma^2_{\mathbf{bb}}$, $\sigma^2_{\mathbf{ss}}$, $\sigma^2_{\boldsymbol{\mu\mu}}$ are the gyro bias, scale factor, and star tracker to gyro misalignment steady-state variances. The matrix $\overline{Q}_k$, on the other hand, can be computed analytically, as done in the next section. This analytical covariance is not used in the on-board filter because of its complexity; however, it is an important tool to evaluate whether the approximated values, used in the filter, are acceptable.

The measurement update is given by

$$\hat{\mathbf{x}}_k^- = \begin{bmatrix} \mathbf{0}^\mathrm{T} & \hat{\mathbf{b}}(t_k)^\mathrm{T} & \hat{\mathbf{s}}(t_k)^\mathrm{T} & \hat{\boldsymbol{\mu}}(t_k)^\mathrm{T} \end{bmatrix}^\mathrm{T} \tag{86}$$

$$\boldsymbol{\epsilon}_k = \mathbf{a}\big(\mathbf{q}_{bi,\,meas}(t_k) \otimes \mathbf{q}(-\hat{\boldsymbol{\mu}}_k) \otimes \hat{\mathbf{q}}^*_{bi}(t_k)\big) \tag{87}$$

$$H = \begin{bmatrix} I_3 & O_3 & O_3 & I_3 \end{bmatrix} \tag{88}$$

$$K_k = P_k^- H^\mathrm{T}\big(HP_k^- H^\mathrm{T} + R_k\big) \tag{89}$$

$$P_k^+ = (I - K_k H)P_k^-(I - K_k H)^\mathrm{T} + K_k R_k K_k^\mathrm{T} \tag{90}$$

$$\begin{bmatrix} \hat{\mathbf{a}}_k^\mathrm{T} & \hat{\mathbf{b}}(t_k)^\mathrm{T} & \hat{\mathbf{s}}(t_k)^\mathrm{T} & \hat{\boldsymbol{\mu}}(t_k)^\mathrm{T} \end{bmatrix}^\mathrm{T} = \hat{\mathbf{x}}_k^- + K_k\boldsymbol{\epsilon}_k \tag{91}$$

$$\hat{\mathbf{q}}_{bi}(t_k) = \mathbf{q}(\hat{\mathbf{a}}_k) \otimes \hat{\mathbf{q}}_{bi}(t_k) \tag{92}$$

where R_k is the star tracker measurement error covariance and $\mathbf{a}(\cdot)$ is the function that returns the three-dimensional attitude parameterization $\mathbf{a}$ from another parameterization such as the quaternion. Our choice of attitude error parameterization is four times the modified Rodrigues parameters [13] which we will refer to as scaled MRPs.

A. The Process Noise Matrix

The mapped process noise matrix, $\overline{Q}_k$ is defined as

$$\overline{Q}_k \triangleq \int_{t_{k-1}}^{t_k} \Phi(t_k,\tau)\, Q\, \Phi^T(t_k,\tau)\, d\tau$$

where the power spectral density Q is

$$Q \triangleq \begin{bmatrix} Q_1 & O_3 & O_3 & O_3 \\ O_3 & Q_2 & O_3 & O_3 \\ O_3 & O_3 & Q_3 & O_3 \\ O_3 & O_3 & O_3 & Q_4 \end{bmatrix} = \begin{bmatrix} Q_1 I_3 & O_3 & O_3 & O_3 \\ O_3 & Q_2 I_3 & O_3 & O_3 \\ O_3 & O_3 & Q_3 I_3 & O_3 \\ O_3 & O_3 & O_3 & Q_4 I_3 \end{bmatrix} \tag{93}$$

Where Q_1 is the per-axis gyro angular random walk and $Q_2 = 2\sigma^2_{\mathbf{bb}}/\tau_b$, $Q_3 = 2\sigma^2_{\mathbf{ss}}/\tau_s$, $Q_4 = 2\sigma^2_{\boldsymbol{\mu\mu}}/\tau_\mu$.

With this in hand, we now will solve for $\overline{Q}_k$, a 16×16 matrix, partitioned into sub-matrices as

$$\overline{Q}_k = \begin{bmatrix} \overline{Q}_{k,11} & \overline{Q}_{k,12} & \overline{Q}_{k,13} & \mathbf{0}_{3\times3} \\ \overline{Q}^T_{k,12} & \overline{Q}_{k,22} & \mathbf{0}_{3\times3} & \mathbf{0}_{3\times3} \\ \overline{Q}^T_{k,13} & \mathbf{0}_{3\times3} & \overline{Q}_{k,33} & \mathbf{0}_{3\times3} \\ \mathbf{0}_{3\times3} & \mathbf{0}_{3\times3} & \mathbf{0}_{3\times3} & \overline{Q}_{k,44} \end{bmatrix} \tag{94}$$

We will solve each of these sub-matrices, $\overline{Q}_{k,11}$, $\overline{Q}_{k,12}$, $\overline{Q}_{k,13}$, $\overline{Q}_{k,22}$, $\overline{Q}_{k,33}$, and $\overline{Q}_{k,44}$ in turn. We begin with $\overline{Q}_{k,11}$, which is

$$\begin{aligned} \overline{Q}_{k,11} &= \overline{Q}_{k,11_a} + \overline{Q}_{k,11_b} + \overline{Q}_{k,11_c} && (95) \\ &= \int_{t_{k-1}}^{t_k} \Phi_{11}(t_k,\tau)\, Q_1\, \Phi^T_{11}(t_k,\tau) + \Phi_{12}(t_k,\tau)\, Q_2\, \Phi^T_{12}(t_k,\tau) + \Phi_{13}(t_k,\tau)\, Q_3\, \Phi^T_{13}(t_k,\tau)\, d\tau && (96) \end{aligned}$$

The first term, $\overline{Q}_{k,11_a}$ is found to be

$$\overline{Q}_{k,11_a} = \int_{t_{k-1}}^{t_k} \Phi_{11}(t_k,\tau)\, Q_1\, \Phi^T_{11}(t,\tau)\, d\tau = Q_1 \Delta t_k\, I_3 \tag{97}$$

The second term, $\overline{Q}_{k,11_b}$ is found to be

$$\begin{aligned} \overline{Q}_{k,11_b} &= \int_{t_{k-1}}^{t_k} \Phi_{12}(t_k,\tau)\, Q_2\, \Phi^T_{12}(t,\tau)\, d\tau && (98) \\ &= Q_2\, \tau^2_{\mathbf{b}_g} \left[-\frac{\tau_{\mathbf{b}_g}}{2} \left(e^{-\frac{2\Delta t_k}{\tau_{\mathbf{b}_g}}} - 1 \right) + 2\tau_{\mathbf{b}_g} \left(e^{-\frac{\Delta t_k}{\tau_{\mathbf{b}_g}}} - 1 \right) + \Delta t_k \right] \left(I_3 + \frac{\omega^2 \tau^2_{\mathbf{b}_g}}{1 + \omega^2 \tau^2_{\mathbf{b}_g}} [\hat{\boldsymbol{\omega}}_m \times]^2 \right) \\ &\quad + [\hat{\boldsymbol{\omega}}_m \times]^2 \left[\frac{2Q_2\, \tau^3_{b_g}}{(1 + \omega^2_m \tau^2_{b_g})^2} \right] \left[e^{-\frac{\Delta t_k}{\tau_{b_g}}} \left(\omega_m \tau_{b_g} \sin \Delta\theta_k - \cos \Delta\theta_k \right) + 1 + (1 + \omega^2_m \tau^2_{b_g})(e^{-\frac{\Delta t_k}{\tau_{b_g}}} - 1) \right] \end{aligned}$$

The third term, $\overline{Q}_{k,11_c}$, is far more complicated and is expressed in Eq. (A1) in the appendix A.

Proceeding along, $\overline{Q}_{k,12}$ is

$$\begin{aligned}
\overline{Q}_{k,12} &= \int_{t_{k-1}}^{t_k} \Phi_{12}(t_k,\tau)\, Q_2\, \Phi_{22}^T(t,\tau)\, d\tau \\
&= Q_2\tau_{b_g}^2 \left[I_3 + \frac{\omega_m \tau_{b_g}[\hat{\boldsymbol{\omega}}_m\times]}{1+\omega_m^2\tau_{b_g}^2}\left(\omega_m\tau_{b_g}[\hat{\boldsymbol{\omega}}_m\times] + I_3\right)\right]\left[-\frac{1}{2}\left(e^{-\frac{2\Delta t_k}{\tau_{b_g}}} - 1\right) + \left(e^{-\frac{\Delta t_k}{\tau_{b_g}}} - 1\right)\right] \\
&\quad + \frac{\tau_{b_g}^2 Q_2[\hat{\boldsymbol{\omega}}_m\times]}{(1+\omega_m^2\tau_{b_g}^2)^2}\left([\hat{\boldsymbol{\omega}}_m\times] - \omega_m\tau_{b_g} I_3\right)\left[e^{-\frac{\Delta t_k}{\tau_{b_g}}}\left(\omega_m\tau_{b_g}\sin\Delta\theta_k + \cos\Delta\theta_k\right) + 1 + \left(1+\omega_m^2\tau_{b_g}^2\right)(e^{-\frac{\Delta t_k}{\tau_{b_g}}} - 1)\right) \\
&\quad - \frac{\tau_{b_g}^2 Q_2[\hat{\boldsymbol{\omega}}_m\times]}{(1+\omega_m^2\tau_{b_g}^2)^2}\left(I_3 + \omega_m\tau_{b_g}[\hat{\boldsymbol{\omega}}_m\times]\right)\left[e^{-\frac{\Delta t_k}{\tau_{b_g}}}\left(\sin\Delta\theta_k + \omega_m\tau_{b_g}\cos\Delta\theta_k\right) - \omega_m\tau_{b_g}\right] \qquad (99)
\end{aligned}$$

Likewise $\overline{Q}_{k,13}$ is

$$\begin{aligned}
\overline{Q}_{k,13} &= \int_{t_{k-1}}^{t_k} \Phi_{13}(t_k,\tau)\, Q_3\, \Phi_{33}^T(t,\tau)\, d\tau \\
&= Q_3\,\tau_{s_g}^2 \left\{ \left[I_3 + \frac{\omega_m \tau_{s_g}[\hat{\boldsymbol{\omega}}_m\times]}{1+\omega_m^2\tau_{b_g}^2}\left(\omega_m\tau_{s_g}[\hat{\boldsymbol{\omega}}_m\times] + I_3\right)\right]\left[-\frac{1}{2}\left(e^{-\frac{2\Delta t_k}{\tau_{s_g}}} - 1\right) + \left(e^{-\frac{\Delta t_k}{\tau_{s_g}}} - 1\right)\right] \right. \\
&\quad + \frac{[\hat{\boldsymbol{\omega}}_m\times]}{(1+\omega_m^2\tau_{s_g}^2)^2}\left([\hat{\boldsymbol{\omega}}_m\times] - \omega_m\tau_{s_g} I_3\right)\left[e^{-\frac{\Delta t_k}{\tau_{s_g}}}\left(\omega_m\tau_{s_g}\sin\Delta\theta_k + \cos\Delta\theta_k\right) + 1 + \left(1+\omega_m^2\tau_{s_g}^2\right)(e^{-\frac{\Delta t_k}{\tau_{s_g}}} - 1)\right) \\
&\quad \left. - \frac{[\hat{\boldsymbol{\omega}}_m\times]}{(1+\omega_m^2\tau_{s_g}^2)^2}\left(I_3 + \omega_m\tau_{s_g}[\hat{\boldsymbol{\omega}}_m\times]\right)\left[e^{-\frac{\Delta t_k}{\tau_{s_g}}}\left(\sin\Delta\theta_k + \omega_m\tau_{s_g}\cos\Delta\theta_k\right) - \omega_m\tau_{s_g}\right]\right\}[\boldsymbol{\omega}_m\backslash] \qquad (100)
\end{aligned}$$

We find that $\overline{Q}_{k,22}$ is

$$\overline{Q}_{k,22} = \int_{t_{k-1}}^{t_k} \Phi_{22}(t_k,\tau)\, Q_2\, \Phi_{22}^T(t,\tau)\, d\tau = \frac{Q_2\tau_{\mathbf{b}_g}}{2}\left(1 - e^{-\frac{2\Delta t_k}{\tau_{\mathbf{b}_g}}}\right) I_3 \qquad (101)$$

Likewise. $\overline{Q}_{k,33}$ is

$$\overline{Q}_{k,33} = \int_{t_{k-1}}^{t_k} \Phi_{33}(t_k,\tau)\, Q_3\, \Phi_{33}^T(t,\tau)\, d\tau = \frac{Q_3\tau_{\mathbf{b}_g}}{2}\left(1 - e^{-\frac{2\Delta t_k}{\tau_{\mathbf{b}_g}}}\right) I_3 \qquad (102)$$

Finally, $\overline{Q}_{k,44}$ is

$$\overline{Q}_{k,44} = \int_{t_{k-1}}^{t_k} \Phi_{44}(t_k,\tau)\, Q_4\, \Phi_{44}^T(t,\tau)\, d\tau = \frac{Q_4\tau_{\alpha_{ST}}}{2}\left(1 - e^{-\frac{2\Delta t_k}{\tau_{\alpha_{ST}}}}\right) I_3 \qquad (103)$$

The complete analytical process noise matrix described above which involve $\sin\Delta\theta_k$ and $\cos\Delta\theta_k$ are computationally expensive to evaluate at each propagation step. To obviate this, it is also possible to approximate

the process noise matrix as follows:

$$\overline{Q}_{k,11} = Q_1\,\Delta t_k\,I_3 + Q_2\,\tau_{\mathbf{b}_g}^2\left[-\frac{\tau_{\mathbf{b}_g}}{2}\left(e^{-\frac{2\Delta t_k}{\tau_{\mathbf{b}_g}}}-1\right)+2\tau_{\mathbf{b}_g}\left(e^{-\frac{\Delta t_k}{\tau_{\mathbf{b}_g}}}-1\right)+\Delta t_k\right]I_3 + Q_3\,\tau_{s_g}^2\left[-\frac{\tau_{s_g}}{2}\left(e^{-\frac{2\Delta t_k}{\tau_{\mathbf{b}_g}}}-1\right)+2\tau_{s_g}\left(e^{-\frac{\Delta t_k}{\tau_{\mathbf{b}_g}}}-1\right)+\Delta t_k\right]\left[\boldsymbol{\omega}_m\backslash\right]^2 \tag{104}$$

$$\overline{Q}_{k,12} = Q_2\,\tau_{b_g}^2\left[-\frac{1}{2}\left(e^{-\frac{2\Delta t_k}{\tau_{b_g}}}-1\right)+\left(e^{-\frac{\Delta t_k}{\tau_{b_g}}}-1\right)\right]I_3 \tag{105}$$

$$\overline{Q}_{k,13} = Q_3\,\tau_{s_g}^2\left[-\frac{1}{2}\left(e^{-\frac{2\Delta t_k}{\tau_{s_g}}}-1\right)+\left(e^{-\frac{\Delta t_k}{\tau_{s_g}}}-1\right)\right]\left[\boldsymbol{\omega}_m\backslash\right] \tag{106}$$

$$\overline{Q}_{k,22} = \frac{Q_2\,\tau_{\mathbf{b}_g}}{2}\left(1-e^{-\frac{2\Delta t_k}{\tau_{\mathbf{b}_g}}}\right)I_3 \tag{107}$$

$$\overline{Q}_{k,33} = \frac{Q_3\,\tau_{\mathbf{b}_g}}{2}\left(1-e^{-\frac{2\Delta t_k}{\tau_{\mathbf{b}_g}}}\right)I_3 \tag{108}$$

$$\overline{Q}_{k,44} = \frac{Q_4\,\tau_{\alpha_{ST}}}{2}\left(1-e^{-\frac{2\Delta t_k}{\tau_{\alpha_{ST}}}}\right)I_3 \tag{109}$$

VI. Numerical Example

This section presents the results of a Monte Carlo simulation used to test the proposed design. The initial attitude uncertainty standard deviation is 0.033 deg, in order to simulate the effects of long coast flights prior to measurement acquisition, the initial attitude estimation error is correlated to the initial gyro bias estimation error with a correlation coefficient $\rho_{\phi b} = -0.9$. The simulation runs for 500 seconds, for the first 200 seconds the vehicle is coasting, the estimation algorithm starts processing star tracker measurements after 100 seconds and continues until the end. At 200 seconds the vehicle starts rolling at a rate of 1 deg/s. At 300 seconds the vehicle stops rolling and starts pitching at a rate of 1 deg/s. At 400 seconds the vehicle returns to coast flight. The star tracker and gyro errors used in the simulation are the same shown in Table 1 (all values are 1σ per axis). Figs. 4 and 5 show the performance of the filter. It can be seen that the actual errors match the uncertainty predicted by the filter.

When star tracker measurements become available at 100 seconds of simulation time the star tracker misalignment errors collapse to the attitude knowledge uncertainty and the two are negatively correlated. There is no noticeable improvement in attitude knowledge because the information is used to estimate the misalignment. Only a slight improvement (less than 0.01 degree) in gyro bias error is observed (best seen in the Y-axis) despite the fact that the gyro bias is observable. Initially, when the gyro bias and the star tracker misalignment are uncorrelated the star tracker misalignment error is quite large (on the order of 1 degree), thereby reducing the gain corresponding to these states. As the attitude error decreases during

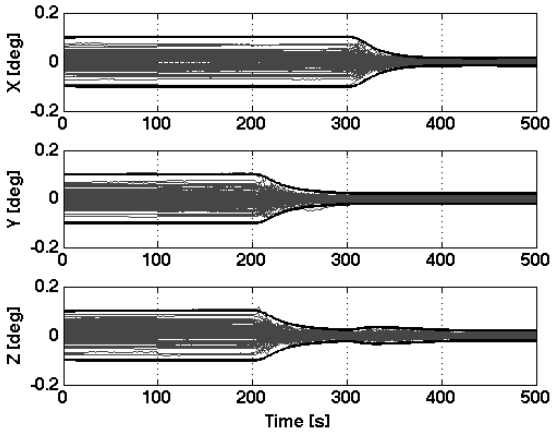

(a) Attitude Error and 3σ Predicted Uncertainty

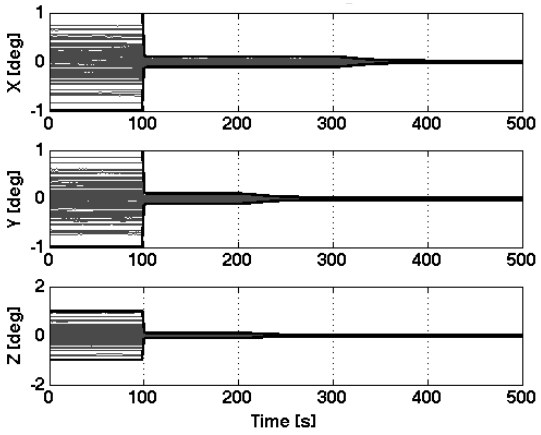

(b) Misalignment Error and 3σ Predicted Uncertainty

Fig. 4 Attitude and Misalignment Estimation Errors, 100 Monte Carlo Runs

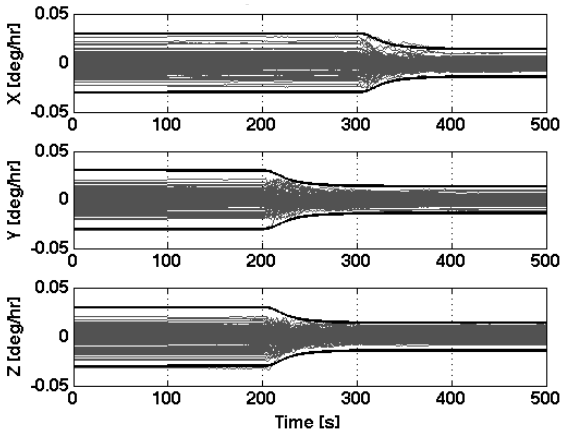

(a) Gyro Bias Error and 3σ Predicted Uncertainty

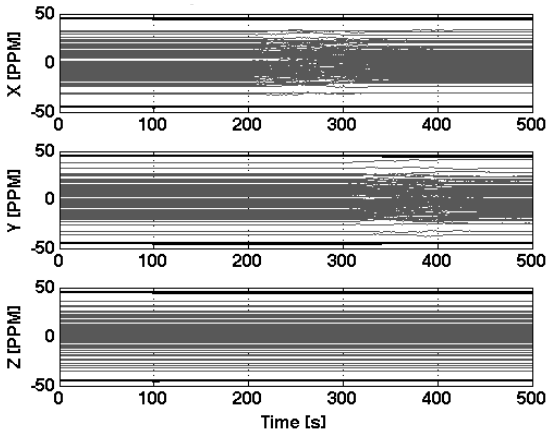

(b) Gyro Scale Factor Error and 3σ Predicted Uncertainty

Fig. 5 Gyro Estimation Errors, 100 Monte Carlo Runs

slews, so does the gyro bias steady state value. The results show that the gyro scale factor uncertainty is not decreasing, as expected, however the state is important to correctly condition the covariance since it is a significant contributor to the total attitude error. Detailed analysis of gyro calibration maneuvers, persistence of excitation conditions, and analysis of convergence can be found in reference [10].

VII. Conclusions

The design for the Orion Attitude Filter is being solidified based upon an extensive observability analysis. In particular, the selection of filter states and dynamics has been informed by an analysis of performance during coast and during attitude maneuvers. Filter performance and error budgets analysis have driven the

design to selecting attitude errors, gyro bias, gyro scale factors and star tracker-to-gyro misalignment as elements of the state space to be estimated. The gyro and star tracker parameters are modeled as first-order Gauss-Markov random processes. Insight into the observability of the state-space was gained by performing a detailed analytic observability analysis. Concept of operations are developed based on the results of this observability analysis.

The performance analysis demonstrates that, as expected, during coasts the gyro bias and attitude errors correlate so that when star tracker measurements are processed, the gyro bias is well estimated. Conversely, during attitude maneuvers the gyro scale-factors correlate with attitude errors; however, the estimation of scale-factor errors is slow. Yet, this particular error is a significant contributor to the total attitude errors and hence is included in the filter state space.

References

[1] Crassidis, J. L., Markley, F. L., and Cheng, Y., "Survey of Nonlinear Attitude Estimation Methods," *Journal of Guidance, Control, and Dynamics*, Vol. 30, No. 1, 2007, pp. 12–28, doi: 10.2514/1.22452.

[2] Bar-Itzhack, I. Y. and Oshman, Y., "Attitude Determination from Vector Observations: Quaternion Estimation," *IEEE Transaction on Aerospace and Electronic Systems*, Vol. 21, No. 1, January 1985, pp. 128–135, doi: 10.1109/TAES.1985.310546 .

[3] Lefferts, E. J., Markley, F. L., and Shuster, M. D., "Kalman Filtering for Spacecraft Attitude Estimation," *AIAA Journal of Guidance, Control, and Dynamics*, Vol. 5, No. 5, 1982, pp. 417–429, doi:10.2514/6.1982-70.

[4] Psiaki, M., Martel, F., and Pal, P., "Three-Axis Attitude Determination via Kalman Filtering of Magnetometer Data," *Journal of Guidance, Control, and Dynamics*, Vol. 13, No. 3, 1990, pp. 506–514, doi: 10.2514/3.25364.

[5] Tanygin, S., "Angles Only Three-Axis Attitude Determination," *AIAA/AAS Astrodynamics Specialist Conference*, Keystone, Colorado, August 2–5 2010, AIAA-2006-7826, doi: 10.2514/6.2010-7826.

[6] Keat, J. E., "Analysis of Least-Squares Attitude Determination Routine DOAOP," Tech. Rep. CSC/TM-77/6034, Computer Sciences Corporation, February 1977.

[7] Shuster, M. D., "Kalman Filtering of Spacecraft Attitude and the QUEST Model," *The Journal of the Astronautical Sciences*, Vol. 38, No. 3, July–September 1990, pp. 377–393.

[8] Woffinden, D. and Geller, D., "Observability Criteria for Angles-Only Navigation," *IEEE Transactions on Aerospace and Electronic Systems*, Vol. 45, No. 3, July 2009, pp. 1194–1208, doi: 10.1109/TAES.2009.5259193.

[9] Pittelkau, M. E., "Survey of Calibration Algorithms for Spacecraft Attitude Sensors and Gyros," *Proceedings of the 2007 AAS/AIAA Spaceflight Mechanics Meeting held August 19–23, 2007, Mackinac Island, Michigan*, Vol. 129 of

Advances in the Astronautical Sciences, 2007, pp. 651–705, AAS 07-295.

[10] Thienel, J. K., *Nonlinear Observer/Controller Designs for Spacecraft Attitude Control Systems with Uncalibrated Gyros*, PhD Dissertation, University of Maryland, 2004, http://hdl.handle.net/1903/1401.

[11] Shuster, M. D., "A Survey of Attitude Representations," *The Journal of the Astronautical Sciences*, Vol. 41, No. 4, 1993, pp. 439–517.

[12] Bortz, J. E., "A New Mathematical Formulation for Strapdown Inertial Navigation," *IEEE Transactions on Aerospace and Electronic Systems*, Vol. 7, No. 1, January 1971, pp. 61–66, doi: 10.1109/TAES.1971.310252 .

[13] Markley, F. L., "Attitude Error Representations for Kalman Filtering," *Journal of Guidance, Control, and Dynamics*, Vol. 26, No. 2, 2003, pp. 311–317.

[14] Tapley, B. D., Schutz, B. E., and Born, G. H., *Statistical Orbit Determination*, Elsevier Academic Press, 2004, pp. 172–173.

[15] Davis, M. H. A. and Vinter, R. B., *Stochastic Modelling and Control*, Monographs on Statistics and Applied Probability, Chapman and Hall, 1985, pp. 125–126.

[16] Younes, A. B., Mortari, D., Turner, J. D., and Junkins, J. L., "Attitude Error Kinematics," *Journal of Guidance, Control, and Dynamics*, Vol. 37, No. 1, 2014, pp. 330–336, doi: 10.2514/1.60928.

[17] Markley, F. L. and Crassidis, J. L., *Fundamentals of Spacecraft Attitude Determination and Control*, Space Technology Library, Springer, 2014, p. 258.

APPENDIX A: THE THIRD PROCESS NOISE MATRIX, $\overline{Q}_{k,11_c}$

We are after the following integral, $\overline{Q}_{k,11_c}$. which is

$$\begin{aligned}\overline{Q}_{k,11_c} &= \int_{t_{k-1}}^{t_k} \Phi_{13}(t_k,\tau)\, Q_3\, \Phi_{13}^T(t_k,\tau)\, d\tau = Q_3 \int_{t_{k-1}}^{t_k} \Phi_{13}(t_k,\tau)\, \Phi_{13}^T(t_k,\tau)\, d\tau \qquad \text{(A1)}\\ &= \eta_a \mathbf{W}_1 - \eta_b(\mathbf{W}_2 + \mathbf{W}_2^T) + \eta_c\,(\mathbf{W}_3 + \mathbf{W}_3^T) - \eta_d \mathbf{W}_5 - \eta_e\,(\mathbf{W}_7 + \mathbf{W}_7^T) + \eta_f\, \mathbf{W}_9\end{aligned}$$

where $\eta_a, \ldots, \eta_f$ are described in Eqs. (A11) - (A16) and $\mathbf{W}_1, \ldots, \mathbf{W}_9$ are given by:

$$\mathbf{W}_1 = [\boldsymbol{\omega}_m \backslash]^2 \tag{A2}$$

$$\mathbf{W}_2 = [\boldsymbol{\omega}_m \backslash]^2 [\hat{\boldsymbol{\omega}}_m \times] \tag{A3}$$

$$\mathbf{W}_3 = [\boldsymbol{\omega}_m \backslash]^2 [\hat{\boldsymbol{\omega}}_m \times]^2 \tag{A4}$$

$$\mathbf{W}_4 = [\hat{\boldsymbol{\omega}}_m \times] [\boldsymbol{\omega}_m \backslash]^2 \tag{A5}$$

$$\mathbf{W}_5 = [\hat{\boldsymbol{\omega}}_m \times] [\boldsymbol{\omega}_m \backslash]^2 [\hat{\boldsymbol{\omega}}_m \times] \tag{A6}$$

$$\mathbf{W}_6 = [\hat{\boldsymbol{\omega}}_m \times]^2 [\boldsymbol{\omega}_m \backslash]^2 = \mathbf{W}_3^T \tag{A7}$$

$$\mathbf{W}_7 = [\hat{\boldsymbol{\omega}}_m \times]^2 [\boldsymbol{\omega}_m \backslash]^2 [\hat{\boldsymbol{\omega}}_m \times] \tag{A8}$$

$$\mathbf{W}_8 = [\hat{\boldsymbol{\omega}}_m \times] [\boldsymbol{\omega}_m \backslash]^2 [\hat{\boldsymbol{\omega}}_m \times]^2 \tag{A9}$$

$$\mathbf{W}_9 = [\hat{\boldsymbol{\omega}}_m \times]^2 [\boldsymbol{\omega}_m \backslash]^2 [\hat{\boldsymbol{\omega}}_m \times]^2 \tag{A10}$$

Finally, $\eta_a, \ldots, \eta_f$ are

$$\begin{aligned} \eta_a &= Q_3 \tau_{s_g}^2 \int_{t_{k-1}}^{t_k} \left(e^{-\frac{(\xi - t_0)}{\tau_{\mathbf{b}_g}}} - 1 \right)^2 d\xi \\ &= Q_3 \omega_m^2 \tau_{s_g}^2 \left[-\frac{\tau_{s_g}}{2} \left(e^{-\frac{2\Delta t_k}{\tau_{\mathbf{b}_g}}} - 1 \right) + 2\tau_{s_g} \left(e^{-\frac{\Delta t_k}{\tau_{\mathbf{b}_g}}} - 1 \right) + \Delta t_k \right] \end{aligned} \tag{A11}$$

$$\begin{aligned} \eta_b &= \frac{Q_3 \tau_{s_g}^2}{1 + \omega_m^2 \tau_{s_g}^2} \int_{t_{k-1}}^{t_k} \left[-\omega_m \tau_{s_g} (\cos \Delta\theta - 1) + \sin \Delta\theta + \omega_m \tau_{s_g} \left(e^{-\frac{\Delta t_k}{\tau_{s_g}}} - 1 \right) \right] \left(e^{-\frac{(\xi - t_0)}{\tau_{\mathbf{b}_g}}} - 1 \right) d\xi \\ &= \frac{Q_3 \omega_m^2 \tau_{s_g}^2}{1 + \omega_m^2 \tau_{s_g}^2} \left\{ -\frac{\omega_m \tau_{s_g}^2}{1 + \omega_m^2 \tau_{s_g}^2} \left[e^{-\frac{\Delta t_k}{\tau_{s_g}}} \left(\omega_m \tau_{s_g} \sin \Delta\theta_k - \cos \Delta\theta_k + 1 + \omega_m^2 \tau_{s_g}^2 \right) - \omega_m^2 \tau_{s_g}^2 \right] \right. \\ &\quad + \tau_{s_g} \sin \omega \Delta t_k - \frac{\tau_{s_g}}{1 + \omega_m^2 \tau_{s_g}^2} \left[e^{-\frac{\Delta t_k}{\tau_{s_g}}} (\sin \Delta\theta_k + \omega\tau \cos \Delta\theta_k) - \omega_m \tau_{s_g} \right] \\ &\quad \left. + \frac{1}{\omega_m} (\cos \Delta\theta_k - 1) - \frac{\omega_m \tau_{s_g}^2}{2} \left(e^{-\frac{2\Delta t_k}{\tau_{s_g}}} - 1 \right) + 2\omega_m \tau_{s_g}^2 \left(e^{-\frac{\Delta t_k}{\tau_{s_g}}} - 1 \right) \right\} \end{aligned} \tag{A12}$$

$$\begin{aligned} \eta_c &= \frac{Q_3 \tau_{s_g}^2}{1 + \omega_m^2 \tau_{s_g}^2} \int_{t_{k-1}}^{t_k} \left[(\cos \Delta\theta - 1) + \omega_m \tau_{s_g} \sin \Delta\theta + \omega_m^2 \tau_{s_g}^2 \left(e^{-\frac{\Delta t_k}{\tau_{s_g}}} - 1 \right) \right] \left(e^{-\frac{(\xi - t_0)}{\tau_{\mathbf{b}_g}}} - 1 \right) d\xi \\ &= \frac{Q_3 \omega_m^2 \tau_{s_g}^2}{1 + \omega_m^2 \tau_{s_g}^2} \left\{ \frac{\tau_{s_g}}{1 + \tau_{s_g}^2 \omega_m^2} \left[e^{-\frac{\Delta t_k}{\tau}} \left(\omega_m \tau_{s_g} \sin \Delta\theta_k - \cos \Delta\theta_k + 1 + \omega_m^2 \tau_{s_g}^2 \right) - \omega_m^2 \tau_{s_g}^2 \right] \right. \\ &\quad - \frac{1}{\omega_m} \sin \Delta\theta_k + \Delta t_k - \frac{\omega_m \tau_{s_g}^2}{1 + \omega_m^2 \tau_{s_g}^2} \left[e^{-\frac{\Delta t_k}{\tau_{s_g}}} \left(\sin \Delta\theta_k + \omega_m \tau_{s_g} \cos \Delta\theta_k \right) - \omega_m \tau_{s_g} \right] \\ &\quad \left. + \tau_{s_g} (\cos \omega \Delta t_k - 1) - \frac{\omega_m^2 \tau_{s_g}^3}{2} \left(e^{-\frac{2\Delta t_k}{\tau_{s_g}}} - 1 \right) + 2\omega_m^2 \tau_{s_g}^3 \left(e^{-\frac{\Delta t_k}{\tau_{s_g}}} - 1 \right) + \omega_m^2 \tau_{s_g}^2 \Delta t_k \right\} \end{aligned} \tag{A13}$$

$$
\begin{aligned}
\eta_d &= \frac{Q_3\tau_{s_g}^2}{(1+\omega_m^2\tau_{s_g}^2)^2}\int_{t_{k-1}}^{t_k}\left[-\omega_m\tau_{s_g}(\cos\Delta\theta-1)+\sin\Delta\theta+\omega_m\tau_{s_g}\left(e^{-\frac{\Delta t_k}{\tau_{s_g}}}-1\right)\right]^2 d\xi \\
&= \frac{Q_3\omega_m^2\tau_{s_g}^2}{(1+\omega_m^2\tau_{s_g}^2)^2}\left\{\omega_m^2\tau_{s_g}^2\left[\frac{1}{2\omega_m}\left(\Delta\theta_k+\frac{1}{2}\sin 2\Delta\theta_k\right)-\frac{2}{\omega_m}\sin\Delta\theta_k+\Delta t_k\right]\right. \\
&\quad +\frac{1}{2\omega_m}\left(\Delta\theta_k-\frac{1}{2}\sin 2\Delta\theta_k\right)+\omega_m^2\tau_{s_g}^2\left[-\frac{\tau_{s_g}}{2}\left(e^{-\frac{2\Delta t_k}{\tau_{s_g}}}-1\right)+2\tau_{s_g}\left(e^{-\frac{\Delta t_k}{\tau_{s_g}}}-1\right)+\Delta t_k\right] \\
&\quad -2\omega_m\tau_{s_g}\left[-\frac{1}{4\omega_m}\left(\cos 2\omega_m\Delta t_k-1\right)+\frac{1}{\omega_m}\left(\cos\omega_m\Delta t_k-1\right)\right]+2\tau_{s_g}\left(\cos\Delta\theta_k-1\right) \\
&\quad -\frac{2\omega_m\tau_{s_g}^2}{1+\tau_{s_g}^2\omega_m^2}\left[e^{-\frac{\Delta t_k}{\tau_{s_g}}}\left(\sin\Delta\theta_k+\omega_m\tau_{s_g}\cos\Delta\theta_k\right)-\omega_m\tau\right]+2\omega_m\tau_{s_g}^2\sin\Delta\theta_k-2\omega_m^2\tau^2\Delta t_k \\
&\quad \left.-\frac{2\omega_m^2\tau_{s_g}^3}{1+\tau_{s_g}^2\omega_m^2}\left[e^{-\frac{\Delta t_k}{\tau_{s_g}}}\left(\omega_m\tau_{s_g}\sin\Delta\theta_k-\cos\Delta\theta_k+1+\omega_m^2\tau_{s_g}^2\right)-\omega_m^2\tau_{s_g}^2\right]\right\} \qquad \text{(A14)}
\end{aligned}
$$

$$
\begin{aligned}
\eta_e &= \frac{Q_3\tau_{s_g}^2}{(1+\omega_m^2\tau_{s_g}^2)^2}\int_{t_{k-1}}^{t_k}\left[-\omega_m\tau_{s_g}(\cos\Delta\theta-1)+\sin\Delta\theta+\omega_m\tau_{s_g}\left(e^{-\frac{\Delta t_k}{\tau_{s_g}}}-1\right)\right] \\
&\qquad\qquad \left[(\cos\Delta\theta-1)+\omega_m\tau_{s_g}\sin\Delta\theta+\omega_m^2\tau_{s_g}^2\left(e^{-\frac{\Delta t_k}{\tau_{s_g}}}-1\right)\right]d\xi \\
&= \frac{Q_3\omega_m^2\tau_{s_g}^2}{(1+\omega_m^2\tau_{s_g}^2)^2}\left\{-\frac{\tau_{s_g}}{2}\left(\omega_m\Delta t_k+\frac{1}{2}\sin 2\omega_m\Delta t_k\right)+2\tau_{s_g}\sin\omega\Delta t_k-\omega_m\tau_{s_g}\Delta t\right. \\
&\quad +\left(1-\omega_m^2\tau_{s_g}^2\right)\left[-\frac{1}{4\omega_m}\left(\cos 2\Delta\theta_k-1\right)+\frac{1}{\omega_m}\left(\cos\Delta\theta_k-1\right)\right] \\
&\quad +\frac{\tau_{s_g}}{2}\left(\Delta\theta_k-\frac{1}{2}\sin 2\Delta\theta_k\right)+\omega_m^3\tau_{s_g}^3\left[-\frac{\tau_{s_g}}{2}\left(e^{-\frac{2\Delta t_k}{\tau_{s_g}}}-1\right)+2\tau_{s_g}\left(e^{-\frac{\Delta t_k}{\tau_{s_g}}}-1\right)+\Delta t_k\right] \\
&\quad +\frac{\omega_m\tau_{s_g}^2(1-\omega_m^2\tau_{s_g}^2)}{1+\tau_{s_g}^2\omega_m^2}\left[e^{-\frac{\Delta t_k}{\tau_{s_g}}}\left(\omega_m\tau_{s_g}\sin\Delta\theta_k-\cos\Delta\theta_k+1+\omega_m^2\tau_{s_g}^2\right)-\omega_m^2\tau_{s_g}^2\right] \\
&\quad -\tau_{s_g}(1-\omega_m^2\tau_{s_g}^2)\left(\sin\omega_m\Delta t_k-\omega_m\Delta t_k\right)+\frac{2\omega_m\tau_{s_g}^2}{\omega}\left(\cos\omega_m\Delta t_k-1\right) \\
&\quad \left.-\frac{2\omega_m^2\tau_{s_g}^3}{1+\tau_{s_g}^2\omega_m^2}\left[e^{-\frac{\Delta t_k}{\tau_{s_g}}}\left(\sin\Delta\theta_k+\omega_m\tau_{s_g}\cos\Delta\theta_k\right)-\omega_m\tau_{s_g}\right]\right\} \qquad \text{(A15)}
\end{aligned}
$$

$$
\begin{aligned}
\eta_f &= \frac{Q_3\tau_{s_g}^2}{(1+\omega_m^2\tau_{s_g}^2)^2}\int_{t_{k-1}}^{t_k}\left[(\cos\Delta\theta-1)+\omega_m\tau_{s_g}\sin\Delta\theta+\omega_m^2\tau_{s_g}^2\left(e^{-\frac{\Delta t_k}{\tau_{s_g}}}-1\right)\right]^2 d\xi \\
&= \frac{Q_3\omega_m^2\tau_{s_g}^2}{(1+\omega_m^2\tau_{s_g}^2)^2}\left\{\frac{1}{2\omega_m}\left(3\Delta\theta_k+\frac{1}{2}\sin 2\Delta\theta_k\right)-\frac{2}{\omega_m}\sin\Delta\theta_k\right. \\
&\quad +\frac{\omega_m\tau_{s_g}^2}{2}\left(\Delta\theta_k-\frac{1}{2}\sin 2\Delta\theta_k\right)+\omega_m^4\tau_{s_g}^4\left[-\frac{\tau_{s_g}}{2}\left(e^{-\frac{2\Delta t_k}{\tau_{s_g}}}-1\right)+2\tau_{s_g}\left(e^{-\frac{\Delta t_k}{\tau_{s_g}}}-1\right)+\Delta t_k\right] \\
&\quad +\frac{2\omega_m^2\tau^3}{1+\tau_{s_g}^2\omega_m^2}\left[e^{-\frac{\Delta t_k}{\tau_{s_g}}}\left(\omega_m\tau_{s_g}\sin\Delta\theta_k-\cos\Delta\theta_k+1+\omega_m^2\tau_{s_g}^2\right)-\omega_m^2\tau_{s_g}^2\right]-2\omega_m\tau_{s_g}^2\sin\Delta\theta_k \\
&\quad +2\omega_m^2\tau^2\Delta t_k-\frac{\tau_{s_g}}{2}\left(\cos 2\Delta\theta_k-1\right)+2\tau_{s_g}\left(\cos\Delta\theta_k-1\right) \\
&\quad \left.-\frac{2\omega_m^3\tau_{s_g}^4}{1+\tau_{s_g}^2\omega_m^2}\left[e^{-\frac{\Delta t_k}{\tau_{s_g}}}\left(\sin\Delta\theta_k+\omega_m\tau_{s_g}\cos\Delta\theta_k\right)-\omega_m\tau_{s_g}\right]-2\omega_m^2\tau_{s_g}^3\left(\cos\Delta\theta_k-1\right)\right\} \qquad \text{(A16)}
\end{aligned}
$$